

Lehigh University

Lehigh Preserve

Theses and Dissertations

1-1-2018

Graphical User Interface for Robust Control Education Based on 3DOF Helicopter System

Shuai Yue

Lehigh University, shuaiyue11@gmail.com

Follow this and additional works at: <https://preserve.lehigh.edu/etd>



Part of the [Mechanical Engineering Commons](#)

Recommended Citation

Yue, Shuai, "Graphical User Interface for Robust Control Education Based on 3DOF Helicopter System" (2018). *Theses and Dissertations*. 5716.

<https://preserve.lehigh.edu/etd/5716>

This Thesis is brought to you for free and open access by Lehigh Preserve. It has been accepted for inclusion in Theses and Dissertations by an authorized administrator of Lehigh Preserve. For more information, please contact preserve@lehigh.edu.

Graphical User Interface for Robust Control Education
Based on 3DOF Helicopter System

by

Shuai Yue

Presented to the Graduate and Research Committee of Lehigh University in
Candidacy for the Degree of Master of Science

in

Mechanical Engineering

Lehigh University

December 2017

Certificate of Approval

This thesis is accepted and approved in partial fulfillment of the requirements for the Master of Science in Mechanical Engineering.

December 1, 2017

Date

Professor Eugenio Schuster
Thesis Advisor

Professor Gary Harlow
Chairperson of Department

Acknowledgements

First of all, I would like to thank my advisor, Professor Eugenio Schuster, who gave me directions and without whom I would not have had the opportunity to do research in such an exciting field. I also want to thank him for providing me the opportunity to work on the helicopter device in the Interdisciplinary Automatic Controls Laboratory (IACL). I would also like to thank PhD candidate Hexiang Wang, who provided technical guidance and a background overview of the theory behind robust control. Finally, I would like to thank my family for their support, particularly my parents who provided financial support while I pursued my MSc. degree.

Contents

Abstract	1
1 Introduction	2
1.1 Robust Control Theory	2
1.2 Definition and Description of the Helicopter	4
1.3 Thesis Proposal	6
2 Schematic of the System	7
2.1 The Helicopter Device	8
2.2 Data Acquisition Device	10
2.3 Joystick	12
3 Mathematical Model	14
3.1 The Euler-Lagrange Method	15
3.2 Nonlinear Model	16
3.3 Linearized State-Space Model	16
3.4 Modeling of the Parametric Uncertainty	18
3.5 Modeling of the Unstructured Uncertainty	23
4 Control Design	25
4.1 General Model	25

4.2	Selecting Weighting Functions	28
5	Software Structure	30
5.1	Initial Condition and Set-point Window	34
5.2	Weighting Functions Window	35
5.3	Model Adjustment Window	35
5.4	Assumptions Check Window	37
5.5	Simulation Window	38
5.6	Experimental Results Window	41
5.7	Robust Stability and Performance Window	41
6	Experimental Demonstrations	45
6.1	Stabilizing the Nominal Plant	45
6.2	Adjusting Mathematical Model	49
6.3	Assessing Robust Stability and Performance	52
7	Conclusion and Future Work	57
7.1	Conclusion	57
7.2	Future Work	58
	Vita	62

List of Tables

3.1 Physical Parameters of the 3 DOF Helicopter Device 16

List of Figures

1.1	Boeing HC-1B Chinook	5
2.1	Connection Diagram of this Control-education Experiment	7
2.2	Helicopter Device	8
2.3	Data Acquisition Device	10
2.4	Terminal Board	11
2.5	Universal Power Module	12
2.6	Joystick	13
3.1	Helicopter Architecture Showing the Three Degrees of Freedom of the System	14
3.2	Additive Uncertainty Model	23
3.3	Multiplicative Input Uncertainty Model	23
3.4	Multiplicative Output Uncertainty Model	24
4.1	S/KS Mixed-sensitivity Minimization in Standard Form	26
4.2	General Control Configuration	27
5.1	Flowchart of the Control-design Process in this GUI	31
5.2	Appearance of the GUI	33
5.3	Structure of Software	33

5.4	Appearance of the Initial Condition and Set-point Window	34
5.5	Appearance of the Weighting Functions Window	35
5.6	Appearance of the Model Adjustment Window	36
5.7	Appearance of the Assumptions Check Window	38
5.8	Appearance of the Simulation Window	38
5.9	Appearance of the Experimental Results Window	41
5.10	$M\Delta$ -Structure for Robust Stability Analysis	42
5.11	$N\Delta$ -Structure for Robust Performance Analysis	43
5.12	Apperance of the Robust Stability and Performance Window	44
6.1	Demo of the Assumptions Check Window	46
6.2	Demo of the Initial Conditions and the Set-points	46
6.3	Linear Dynamic Response Simulation of the First Group	47
6.4	Nonlinear Dynamic Response Simulation of the First Group	47
6.5	Linear Dynamic Response Simulation of the Second Group	48
6.6	Nonlinear Dynamic Response Simulation of the Second Group	48
6.7	Linear Dynamic Response Simulation of the Second Group with $L_a = 25$	49
6.8	Nonlinear Dynamic Response Simulation of the Second Group with $L_a = 25$	49
6.9	Linear Dynamic Response Simulation of the Second Group with $L_a = 23$	50
6.10	Nonlinear Dynamic Response Simulation of the Second Group with $L_a = 23$	50
6.11	Linear Dynamic Response Simulation of the Third Group with $L_a = 23$	51
6.12	Nonlinear Dynamic Response Simulation of the Third group with $L_a = 23$	52
6.13	Linear Dynamic Response Simulation of the Fourth Group	53
6.14	Nonlinear Dynamic Response Simulation of the Fourth Group	53

6.15 μ -analysis Results of the Fourth Group	54
6.16 Linear Dynamic Response Simulation of the Fifth Group	55
6.17 Nonlinear Dynamic Response Simulation of the Fifth Group	55
6.18 μ -analysis Results of the Fifth Group(a)	55
6.19 μ -analysis Results of the Fifth Group(b)	56

Abstract

Robustness is an important characteristic of feedback controllers. Many systems with non-linearities and parameter uncertainties usually require sufficient robustness to stay stable. Robust control education is therefore very important for graduate students. However, many educational programs in robust control are exclusively theoretical. This thesis work aims at designing and developing a user-friendly Graphical User Interface (GUI) based on MATLAB for robust-control education based on a non-linear and highly-coupled helicopter system. Although the control design method is limited to the S/KS mixed-sensitivity method, it offers a convenient and ready-to-use GUI for robust control design, dynamic response simulation, robust stability/robust performance assessment, and control implementation. Users can generate the controller by inputting parameters of two weighting functions. Linear and nonlinear simulations based on a discrete-time model are used to assess performance. Structured singular values are used to assess robust stability and robust performance conditions with three typical types of uncertainty. In the end, the designed controller can be loaded into Simulink to control the actual helicopter device. This robust-control educational experiment offers an easy way to test in practice fundamentals of robust control theory.

Chapter 1

Introduction

This chapter will present an introduction to robust control theory and the helicopter control problem. Two aspects will be discussed:

- Development and history of robust control theory.
- Modeling and analysis of the three-degrees-of-freedom helicopter.

1.1 Robust Control Theory

In the early 1980s, as control theory matured, designers found a precise process model was required when they wanted to design a controller. This requirement is usually too strict because the mathematical model of a real system inevitably has errors. Such errors come from the unknown or partially known parameters in the linear model, the variation of operating conditions, the uncertain disturbance from outside or inside, and missing dynamics that usually happens at higher frequencies. Consequently, when the controller is applied on the real system, the expected performance may not be reached. Considering these disadvantages of control theory, designers started to pay attention to control design problems of uncertain systems. The research in this

area evolves in two ways. One way is to assume that the process parameters are unknown and time-variant. Adopting the separation design principle, designers need to identify the parameters of the process first. Based on this adaptive control theory, self-tuning control [1] and model reference adaptive control [2] was proposed. The second way is to assume that the system is uncertain, but the range of uncertainty is known in advance. The designed controller based on this method can guarantee the real system is stable and will perform well within the uncertainty range. The second method is called robust control theory [3–6], which developed from the 1980s and has been deeply researched. In general, the early 1980s to 1987 was the development period of robust control theory [7]. From the beginning of the 1980s, the robust stable problem of controlled systems attracted research and attention in every special problem domain. For example, in the adaptive control area, robust adaptive control theory was developed [1, 8]. In the optimal control area, robust optimal control theory was developed. In particular, its important to point out that lots of robust-control design problems can be converted into minimizing the H_∞ norm of a closed-loop system transfer function matrix [2, 10–13]. This is an important result in robust control theory, which provides a powerful tool for control analysis and design. Consequently, the concept of robust stability has been broadly studied. It involves control design problems in the frequency domain, time domain, continuous domain and discrete domain. Therefore, it is impossible to summarize all research work on robust control.

Robust control has been established as an important body of control-design theory, especially for complex systems with model uncertainties and high order dynamics. Consequently, research and education on robust control is an important component of any graduate program in controls. This is why the overall goal of this thesis work is to develop a control-design and simulation platform for implementation of robust

control algorithms in a real device (helicopter).

1.2 Definition and Description of the Helicopter

One of the objectives of this thesis is to design a robust controller for an autonomous helicopter. A helicopter is defined as an aircraft where the body is lifted by rotating propellers. Autonomous means that the helicopter can fly by itself without guidance from a human being. The most common helicopters consist of two rotors, a main rotor and a tail rotor. The main rotor provides the vertical thrust and the tail rotor provides a horizontal thrust that counters the torque induced by the main rotor [14]. In this thesis, the helicopter that is modeled is a Boeing HC-1B Chinook as shown in Fig. 1.1. This tandem rotor multi-functional helicopter has two engines and two propellers and is mainly used for transport. The contra-rotating rotors structure gets rid of the tail rotor. This structure allows the helicopter to lift vertically. One of the advantages of the contra-rotating rotors structure is that the tail rotor is unnecessary for balancing the torques from the main rotor, so that it is more effective than the helicopters with tail rotor. Meanwhile, the disadvantage of this structure is that two propellers must rotate synchronously to avoid a crash. The airflow produced by the superimposed propellers may interrupt each other and lead to power loss. Consequently, only a few kinds of helicopters adopt this structure.



Figure 1.1: Boeing HC-1B Chinook [19]

On the other hand, analyzing three degrees of freedom (DOF) helicopters has attracted lots of attention from researchers [15]. The three DOFs helicopter control system is a nonlinear and highly-coupled multiple-input and multiple-output (MIMO) system with some unknown parameters and unmodeled dynamics. Several electromechanical parameters and physical parameters are not clearly known. Therefore, the anti-jamming ability and stability of this system are weak, which means that in order to control such a system a robust controller must be implemented. Several robust control techniques have been applied to this model, ranging from adaptive control to state-space predictive control [16, 17]. Considering that the H_∞ is a popular methodology in robust-control design, we adopt the H_∞ mixed sensitivity method in this control-education experiment to design a trajectory tracking controllers.

1.3 Thesis Proposal

An easy-to-use and time-saving helicopter experiment is presented for robust control education purposes using a Graphical User Interface (GUI) in Matlab and a helicopter device. The helicopter device, produced by Quanser, has three degrees of freedom and is driven by two motors. Matlab/Simulink provides powerful built-in functions for users to synthesize robust controllers easily and quickly. It is also good at plotting simulation results and communicating with hardware devices. The GUI window designed as part of this thesis allows users to adjust several parameters of the mathematical model, check the simulation results, assess the robust stability, and send voltage signals from and to the helicopter through a data acquisition device. The goal of this control-education experiment is to design a robust controller by the H_∞ method, which can stabilize this helicopter device in theory based on the model, and can be implemented on helicopter device to verify the robust stability in practice.

The outline of this thesis is stated below. Chapter 2 describes components of the close-loop system, including mechanical components and hardware. Chapter 3 describes the mathematical model of the helicopter device and derives state-space model. Chapter 4 describes the control-design method. Chapter 5 illustrates the software program structure and the functions on the graphical user interface. Chapter 6 presents experimental demonstrations using this GUI and Chapter 7 concludes the thesis.

Chapter 2

Schematic of the System

This chapter will introduce the hardware devices of the robust control education system. This robust control education system is composed of a helicopter device from Quanser, a data acquisition (DAQ) card to communicate between a computer and the helicopter, a joystick from Logitech and a Graphical User Interface (GUI) designed in MATLAB for students to operate. The connection of hardwares is shown in Fig. 2.1.

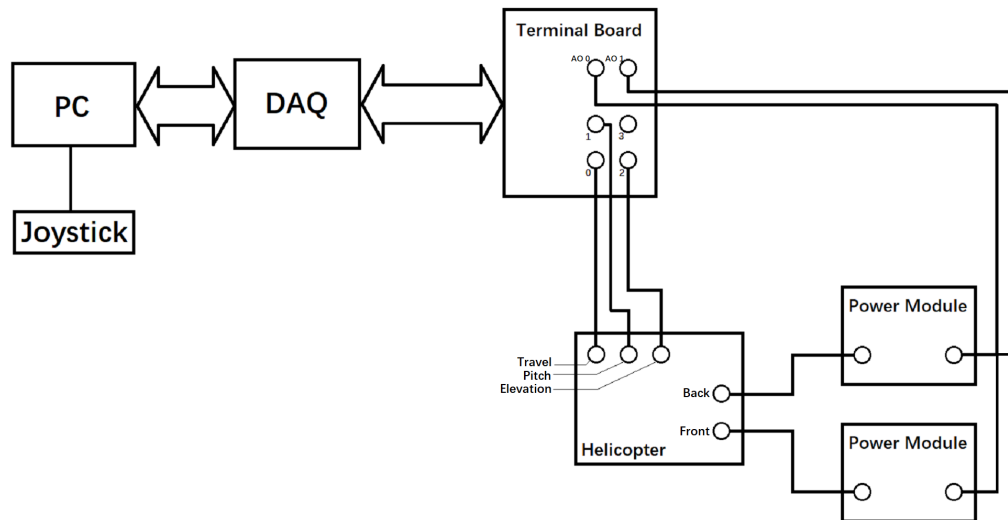


Figure 2.1: Connection Diagram of this Control-education Experiment

2.1 The Helicopter Device

The helicopter device shown in Fig. 2.2, which simulates the Boeing HC-1B Chinook, basically consists of a level, a counterweight and two direct-current motors. The counterweight and the helicopter body, which is a small arm with one rotor at each end, are installed on each end of the level. Two motors can lift the beam to rotate around a pivot. The pose of this system can be described by three angles which are named elevation, pitch and travel. These angles are measured by two incremental encoders and a slip ring. Although this system cannot move in three directions freely, it can rotate about three axes freely.



Figure 2.2: Helicopter Device [19]

The weight of the counterweight block is 1.87 kilograms. The distance between the center of counterweight and the pivot of the level can be adjusted by dismantling the screw on the counterweight and installing it in other positions. However, dismantling and mounting the counterweight consumes significant time and effort. In order to save time, students are not suggested to move the position of the counterweight. In

this control-education experiment, the parameters of the mathematical model can be adjusted according to the actual configuration (this topic will be discussed in Chapter 5). In addition, the distance between the body of helicopter and the pivot of the level can be adjusted as well.

The direct-current motor is a Pittman 9234S004-R1 servo motor. This is a brush commutated motor and the nominal voltage of this motor is 12 volts. It drives a propeller that has three blades. In our control-education experiment, it is assumed that the force-thrust constant of the propeller is 0.1188 Newton per Volt. This constant value is found experimentally. The real force-thrust value may vary with the operating condition especially at high frequencies. In this control-education experiment, the first uncertainty is introduced by using this approximate value in our simplified system model.

The incremental encoder is a two-channel optimal incremental encoder module. The HEDS-9000 series are high performance, low cost, optical incremental encoder modules. When used with a code-wheel, these modules can detect rotary position. These modules consist of a lensed source and an ion chromatography detector enclosed in a small C-shaped plastic package. Due to a highly-collimated light source and unique photo-detector array, these modules are extremely tolerant to mounting misalignment. The slip ring is for measuring the value of the travel angle. It has the same function as the incremental encoder. The resolution of the pitch and the elevation encoder is $2 \times \pi / (4 \times 1024)$ rad per count and the resolution of the travel encoder is $2 \times \pi / (8 \times 1024)$ rad per count.

2.2 Data Acquisition Device

To communicate between the computer and the helicopter, a data acquisition (DAQ) card, a terminal board and a universal power module are installed, which are utilized to transfer voltage signals to the motors and receive pulsing signals from the encoders as well. The DAQ hardware acts as an interface between the computer and signals from outside. It primarily functions as a device that digitizes incoming analog signals so that a computer can interpret them. The three key components of a DAQ device used for measuring a signal are the signal conditioning circuitry, analog-to-digital converter (ADC), and computer bus. Many DAQ devices include other functions for automating measurement systems and processes. For example, digital-to-analog converters (DACs) output analog signals, digital I/O lines input and output digital signals, and counter/timers count and generate digital pulses.

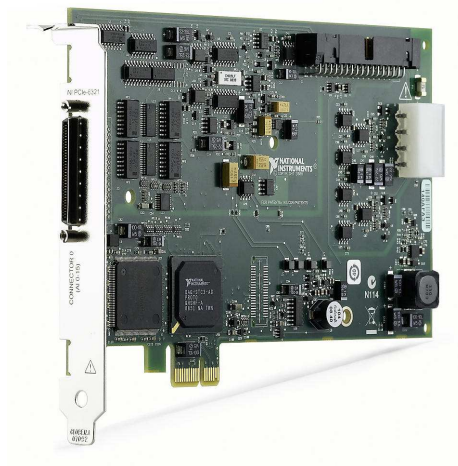


Figure 2.3: Data Acquisition Device [20]

The DAQ card we used in this robust control education system is a PCIe-6321 board produced by National Instrument as shown in Fig. 2.3, and it has two analog output ports for the rotors. The maximum value of the analog output port is 10v. However, the voltage signals from the DAQ will be amplified by two universal power

modules in order to meet the requirements of the motors and the gain is 5. Therefore the output signals to the motors are restricted to under 2.4V. The DAQ card also has three 32-bit counters/timers for the encoders, which are fast enough to generate 1 to 10 microsecond sampling time for real-time control purposes.

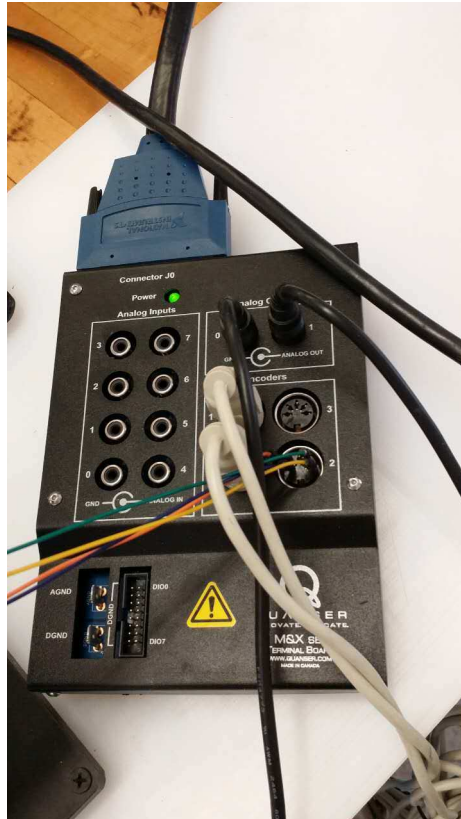


Figure 2.4: Terminal Board

The terminal board shown in Fig. 2.4 is a connector which allows more than one circuit to connect to another circuit. Our terminal board has a 68 pin male interface to connect to the DAQ, three 5-pin interfaces for the encoders and two analog output interfaces for the universal power modules. The universal power modules are shown in Fig. 2.5



Figure 2.5: Universal Power Module

2.3 Joystick

A joystick is an input device consisting of a stick that pivots on a base and reports its angle or direction to the device it is controlling. A joystick, also known as the control column, is the principal control device in the cockpit of many civilian and military aircrafts, either as a center stick or a side-stick. It often has supplementary switches to control various aspects of the aircraft's flight.

The joystick we used in this robust control education system is a Attack 3 from Logitech as shown in Fig. 2.6. The pose of the helicopter device can be set by three angles or it can be controlled by the joystick. Although there are lots of buttons on the joystick, only the stick to control the position of the helicopter is used in this

experiment. Pushing the stick forward decreases the elevation angle and pulling the stick increases the elevation angle. In addition, pushing the stick to left side increases the travel angle and pushing to right side decreases the travel angle.



Figure 2.6: Joystick [21]

Chapter 3

Mathematical Model

This helicopter system has three degrees of freedom around the elevation-axis, pitch-axis and travel-axis. The helicopter system architecture is shown in Fig. 3.1.

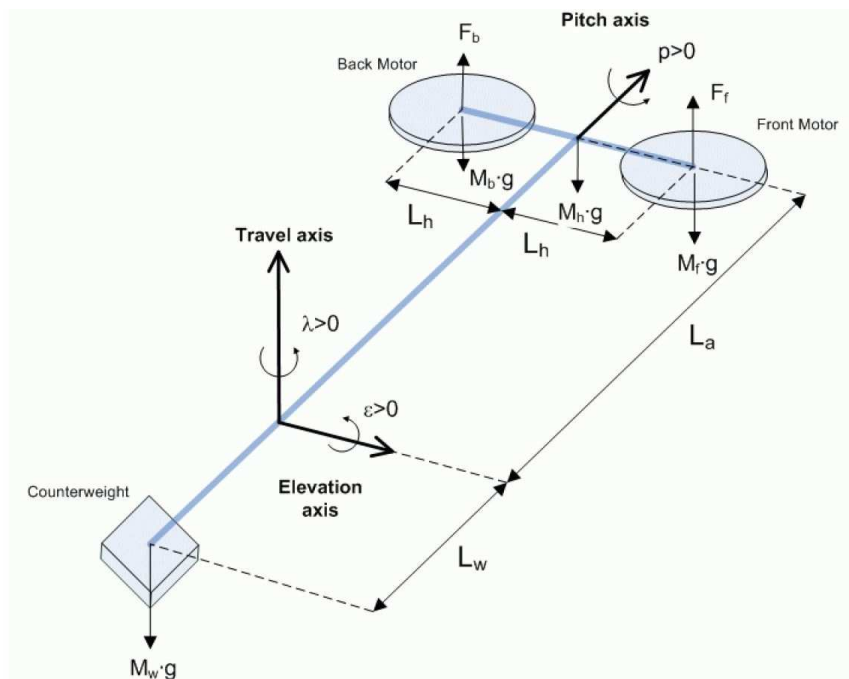


Figure 3.1: Helicopter Architecture Showing the Three Degrees of Freedom of the System [19]

The pitch of the helicopter is the rotation around an axis parallel to the level.

The elevation axis is defined as an axis parallel to the helicopter body, at the base coordinate frame. The travel axis is defined as a vertical line at the base coordinate frame perpendicular to the elevation axis.

- The helicopter is horizontal when the elevation angle equals $\epsilon = 0$.
- The travel angle increases positively, $\lambda(t) > 0$, when the body rotates in the counter-clockwise (CCW) direction.
- The pitch angle is positive, $\rho(t) > 0$, when the front motor is higher than the back motor.

3.1 The Euler-Lagrange Method

The Euler-Lagrange equation, or Lagrange's equation, is a fundamental equation in multi-body dynamics. It was developed by Swiss mathematician Leonhard Euler and Italian-French mathematician Joseph-Louis Lagrange in the 1750s. When compared with the classical mechanics, the Euler-Lagrange equation is equal to Newton's law of motion, but it has an advantage in that it takes the same form in any system of generalized coordinates.

The Euler-Lagrange equation in mechanics is given by

$$\frac{d}{dt} \left(\frac{\partial T}{\partial \dot{q}_j} \right) - \frac{\partial T}{\partial q_j} = Q_j \quad (j = 1, 2, \dots, k), \quad (3.1)$$

where T is the kinetic energy with respect to the generalized coordinate q_j and the generalized velocity \dot{q}_j , and where Q_j are the generalized forces with respect to q_j .

3.2 Nonlinear Model

By using the Euler-Lagrange method, the nonlinear equations of motion of the 3 DOF helicopter system can be derived. The angular acceleration components are

$$\begin{cases} \ddot{\epsilon} = \frac{L_a K_f}{2m_f(L_a^2 + L_h^2 \sin(\rho)^2) + m_w L_w^2} (u_1 + u_2) \cos(\rho) \\ \ddot{\rho} = \frac{K_f}{2m_f L_h} (u_1 - u_2) \\ \ddot{\lambda} = \frac{(2L_a m_f - L_w m_w)g}{2m_f(L_a^2 \cos(\epsilon)^2 + L_h^2 \sin(\rho)^2 \sin(\epsilon)^2 + L_h^2 \cos(\rho)^2) + m_w L_w^2 \cos(\epsilon)^2} \tan(\rho) \end{cases} \quad (3.2)$$

and the symbols used in Eqs. (3.2) are described in Table 3.1.

Symbol	Unit	Description
u_1	Volt	Voltage applied to the front motor
u_2	Volt	Voltage applied to the back motor
m_f	kg	Mass of front propeller assembly = motor + shield + propeller + body
m_w	kg	Mass of the front section of the helicopter
L_a	m	The distance from the pivot point to the helicopter body
L_w	m	The distance from the pivot point to the counterweight
L_h	m	The distance from the pitch axis to either motor
K_f	N/V	Propeller force-thrust constant found experimentally

Table 3.1: Physical Parameters of the 3 DOF Helicopter Device

3.3 Linearized State-Space Model

Since the H_∞ robust-control method requires a linear model to represent the system, the nonlinear mathematical model must be linearized around an equilibrium point. Here we assume that the equilibrium point occurs at the horizontal position, which

means that the elevation angle ϵ and the pitch angle ρ are both approximately zero. Thus, $\sin(\rho) \approx 0$, $\cos(\rho) \approx 1$, $\sin(\epsilon) \approx 0$, $\cos(\epsilon) \approx 1$, and $\tan(\rho) \approx \rho$. The linear state-space model

$$\begin{aligned} \dot{x} &= Ax + Bu \\ y &= Cx + Du \end{aligned} \tag{3.3}$$

is obtained by linearizing the nonlinear dynamics around the $\epsilon = \rho = 0$.

The state vector for the 3 DOF is defined as the Eq. (3.4):

$$x^T = [\epsilon, \rho, \lambda, \frac{d}{dt}\epsilon, \frac{d}{dt}\rho, \frac{d}{dt}\lambda]. \tag{3.4}$$

The output vector is

$$y^T = [\epsilon, \rho, \lambda],$$

and the input vector is

$$u^T = [V_f, V_b],$$

where V_f is the voltage signal to the front rotor and V_b is the voltage signal to the back rotor.

The corresponding helicopter state-space matrices are

$$\bar{A} = \begin{bmatrix} 0 & 0 & 0 & 1 & 0 & 0 \\ 0 & 0 & 0 & 0 & 1 & 0 \\ 0 & 0 & 0 & 0 & 0 & 1 \\ 0 & 0 & 0 & 0 & 0 & 0 \\ 0 & 0 & 0 & 0 & 0 & 0 \\ 0 & -\frac{(L_w \bar{m}_w - 2L_a \bar{m}_f)g}{\bar{m}_w L_w^2 + 2m_f L_h^2 + 2m_f L_a^2} & 0 & 0 & 0 & 0 \end{bmatrix}$$

$$\begin{aligned}
\bar{B} &= \begin{bmatrix} 0 & 0 \\ 0 & 0 \\ 0 & 0 \\ \frac{\bar{L}_a K_f}{2m_f \bar{L}_a^2 + \bar{m}_w \bar{L}_w^2} & \frac{\bar{L}_a K_f}{2m_f \bar{L}_a^2 + \bar{m}_w \bar{L}_w^2} \\ \frac{K_f}{2m_f L_h} & -\frac{K_f}{2m_f L_h} \\ 0 & 0 \end{bmatrix} \\
C &= \begin{bmatrix} 1 & 0 & 0 & 0 & 0 & 0 \\ 0 & 1 & 0 & 0 & 0 & 0 \\ 0 & 0 & 1 & 0 & 0 & 0 \end{bmatrix}, \text{ and} \\
D &= \begin{bmatrix} 0 & 0 \\ 0 & 0 \\ 0 & 0 \end{bmatrix}, \tag{3.5}
\end{aligned}$$

where \bar{L}_a , \bar{L}_w and \bar{m}_w are the nominal values of the corresponding parameters.

3.4 Modeling of the Parametric Uncertainty

As mentioned in section 2.1, a model modification window is designed for users to adjust some parameters in the mathematical model in order to represent parametric uncertainty. If the parameters of the mathematical model are changed, these parameters on the actual system become the ‘error’ one.

$$L_a = \bar{L}_a(1 + P_{L_a}\delta) \quad L_w = \bar{L}_w(1 + P_{L_w}\delta) \quad m_w = \bar{m}_w(1 + P_{m_w}\delta)$$

where P_{L_a} , P_{L_w} , P_{m_w} are the maximum relative uncertainty in each of these physical parameters and δ is any real scalar satisfying $|\delta| \leq 1$. For example, the nominal value

of the distance from the elevation pivot to the helicopter body (L_a) is 26 ft. If this value in the mathematical model is changed from the nominal value to another value, i.e. 22 ft, the $P_{La} = \frac{L_{amax} - \bar{L}_a}{\bar{L}_a} = \frac{26 - 22}{22} \approx 0.18$.

The state-space for the plant with uncertainty is

$$A' = \begin{bmatrix} 0 & 0 & 0 & 1 & 0 & 0 \\ 0 & 0 & 0 & 0 & 1 & 0 \\ 0 & 0 & 0 & 0 & 0 & 1 \\ 0 & 0 & 0 & 0 & 0 & 0 \\ 0 & 0 & 0 & 0 & 0 & 0 \\ 0 & -\frac{(\bar{L}_w \bar{m}_w (1 + P_{mw} \delta)(1 + P_{Lw} \delta) - 2\bar{L}_a (1 + P_{La} \delta) m_f) g}{\bar{m}_w \bar{L}_w^2 (1 + P_{Lw} \delta)^2 (1 + P_{mw} \delta) + 2m_f L_h^2 + 2m_f \bar{L}_a^2 (1 + P_{La} \delta)^2} & 0 & 0 & 0 & 0 \end{bmatrix} \text{ and}$$

$$B' = \begin{bmatrix} 0 & 0 \\ 0 & 0 \\ 0 & 0 \\ \frac{\bar{L}_a K_f (1 + P_{La} \delta)}{2m_f \bar{L}_a^2 (1 + P_{La} \delta)^2 + \bar{m}_w \bar{L}_w^2 (1 + P_{Lw} \delta)^2 (1 + P_{mw} \delta)} & \frac{\bar{L}_a K_f (1 + P_{La} \delta)}{2m_f \bar{L}_a^2 (1 + P_{La} \delta)^2 + \bar{m}_w \bar{L}_w^2 (1 + P_{Lw} \delta)^2 (1 + P_{mw} \delta)} \\ \frac{K_f}{2m_f L_h} & -\frac{K_f}{2m_f L_h} \\ 0 & 0 \end{bmatrix}. \quad (3.6)$$

Matrices C and D are the same as those in the nominal model.

Rewrite matrices \bar{A} and \bar{B} in Eqs. (3.5) as

$$\bar{A} = \begin{bmatrix} 0 & 0 & 0 & 1 & 0 & 0 \\ 0 & 0 & 0 & 0 & 1 & 0 \\ 0 & 0 & 0 & 0 & 0 & 1 \\ 0 & 0 & 0 & 0 & 0 & 0 \\ 0 & 0 & 0 & 0 & 0 & 0 \\ 0 & -\bar{\alpha} & 0 & 0 & 0 & 0 \end{bmatrix} \text{ and}$$

$$\bar{B} = \begin{bmatrix} 0 & 0 \\ 0 & 0 \\ 0 & 0 \\ \bar{\beta}_1 & \bar{\beta}_1 \\ \beta_2 & \beta_2 \\ 0 & 0 \end{bmatrix}$$

where $\bar{\alpha} = \frac{(\bar{L}_w \bar{m}_w - 2\bar{L}_a m_f)g}{\bar{m}_w \bar{L}_w^2 + 2m_f L_h^2 + 2m_f \bar{L}_a^2}$, $\bar{\beta}_1 = \frac{\bar{L}_a K_f}{2m_f \bar{L}_a^2 + \bar{m}_w \bar{L}_w^2}$ and $\beta_2 = \frac{K_f}{2m_f L_h}$.

Matrices A' and B' can also be rewritten as

$$A' = \begin{bmatrix} 0 & 0 & 0 & 1 & 0 & 0 \\ 0 & 0 & 0 & 0 & 1 & 0 \\ 0 & 0 & 0 & 0 & 0 & 1 \\ 0 & 0 & 0 & 0 & 0 & 0 \\ 0 & 0 & 0 & 0 & 0 & 0 \\ 0 & -\alpha' & 0 & 0 & 0 & 0 \end{bmatrix} \text{ and}$$

$$B' = \begin{bmatrix} 0 & 0 \\ 0 & 0 \\ 0 & 0 \\ \beta'_1 & \beta'_1 \\ \beta_2 & \beta_2 \\ 0 & 0 \end{bmatrix}$$

where α' and β'_1 are the parameters with uncertainty. Therefore the transfer function is

$$\begin{aligned} G'_m &= C(sI - A')^{-1}B' \\ &= C \begin{bmatrix} s & 0 & 0 & -1 & 0 & 0 \\ 0 & s & 0 & 0 & -1 & 0 \\ 0 & 0 & s & 0 & 0 & -1 \\ 0 & 0 & 0 & s & 0 & 0 \\ 0 & 0 & 0 & 0 & s & 0 \\ 0 & \alpha' & 0 & 0 & 0 & s \end{bmatrix}^{-1} B' \\ &= C \begin{bmatrix} \frac{1}{s} & 0 & 0 & -\frac{1}{s^2} & 0 & 0 \\ 0 & \frac{1}{s} & 0 & 0 & -\frac{1}{s^2} & 0 \\ 0 & \frac{\alpha'}{s^3} & \frac{1}{s} & 0 & -\frac{\alpha'}{s^4} & -\frac{1}{s^2} \\ 0 & 0 & 0 & \frac{1}{s} & 0 & 0 \\ 0 & 0 & 0 & 0 & \frac{1}{s} & 0 \\ 0 & -\frac{\alpha'}{s^2} & 0 & 0 & \frac{\alpha'}{s^3} & \frac{1}{s} \end{bmatrix} B' \\ &= \begin{bmatrix} -\frac{\beta'_1}{s^2} & -\frac{\beta'_1}{s^2} \\ -\frac{\beta_2}{s^2} & \frac{\beta_2}{s^2} \\ -\frac{\beta_2\alpha'}{s^4} & \frac{\beta_2\alpha'}{s^4} \end{bmatrix}. \end{aligned}$$

The nominal state-space can be written as

$$\overline{G}_m = \begin{bmatrix} -\frac{\bar{\beta}_1}{s^2} & -\frac{\bar{\beta}_1}{s^2} \\ -\frac{\beta_2}{s^2} & \frac{\beta_2}{s^2} \\ -\frac{\beta_2\bar{\alpha}}{s^4} & \frac{\beta_2\bar{\alpha}}{s^4} \end{bmatrix}.$$

The relationship between G'_m and \overline{G}_m is

$$G'_m = (I + \Delta(s))\overline{G}_m \quad (3.7)$$

where $\Delta(s)$ is a description of the uncertainty. Assuming

$$\Delta(s) = \begin{bmatrix} a & b & c \\ l & m & n \\ r & p & q \end{bmatrix},$$

the Eq. (3.6) can be rewritten as

$$\begin{bmatrix} -\frac{\beta'_1}{s^2} & -\frac{\beta'_1}{s^2} \\ -\frac{\beta_2}{s^2} & \frac{\beta_2}{s^2} \\ -\frac{\beta_2\alpha'}{s^4} & \frac{\beta_2\alpha'}{s^4} \end{bmatrix} = \begin{bmatrix} a & b & c \\ l & m & n \\ r & p & q \end{bmatrix} \begin{bmatrix} -\frac{\bar{\beta}_1}{s^2} & -\frac{\bar{\beta}_1}{s^2} \\ -\frac{\beta_2}{s^2} & \frac{\beta_2}{s^2} \\ -\frac{\beta_2\bar{\alpha}}{s^4} & \frac{\beta_2\bar{\alpha}}{s^4} \end{bmatrix}.$$

There are 9 unknowns and 6 equations, thus there are 3 free variables in the solution of $\Delta(s)$. The solution is

$$\Delta(s) = \begin{bmatrix} \frac{\beta'_1}{\beta_1} - 1 & -\frac{c\bar{\alpha}}{s^2} & c \\ 0 & -\frac{n\bar{\alpha}}{s^2} & n \\ 0 & \frac{\alpha' - q\bar{\alpha}}{s^2} & q - 1 \end{bmatrix},$$

where c , n and q are free variables.

3.5 Modeling of the Unstructured Uncertainty

In this control-education experiment, users can choose different types of unstructured uncertainty from three typical types. Additive uncertainty, multiplicative input uncertainty, and multiplicative output uncertainty are alternative options. Their models are shown in Fig. 3.2-Fig. 3.4.

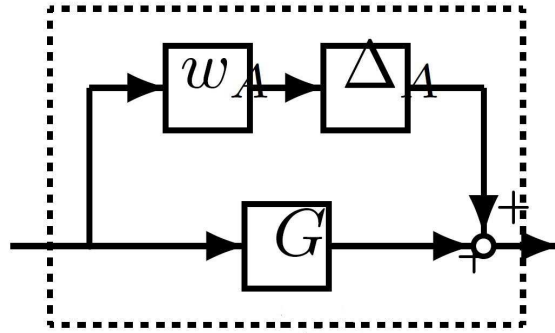


Figure 3.2: Additive Uncertainty Model [22]

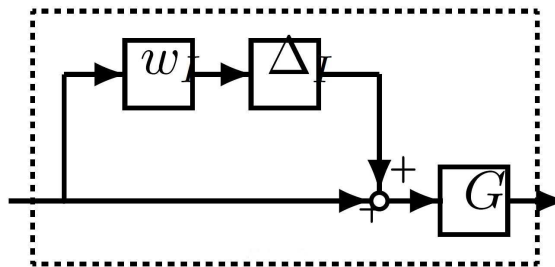


Figure 3.3: Multiplicative Input Uncertainty Model [22]

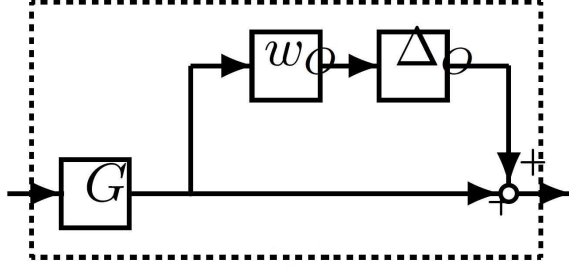


Figure 3.4: Multiplicative Output Uncertainty Model [22]

In many cases, various sources of unstructured uncertainty can be lumped into one form and the equations that represent these forms are:

$$\text{Additive uncertainty} \quad G_p(s) = G(s) + w_A(s)\Delta_a(s) \quad \|\Delta_a\|_\infty \leq 1$$

$$\text{Multiplicative input uncertainty} \quad G_p(s) = G(s)(I + w_I(s)\Delta_I(s)) \quad \|\Delta_I\|_\infty \leq 1$$

$$\text{Multiplicative output uncertainty} \quad G_p(s) = (I + w_O(s)\Delta_O(s))G(s) \quad \|\Delta_O\|_\infty \leq 1$$

where Δ_A , Δ_I or Δ_O are any stable transfer functions that have a magnitude less than or equal to 1 for all frequencies. $w_A(s)$, $w_I(s)$, or $w_O(s)$ are the weighting functions.

Chapter 4

Control Design

This chapter illustrates the general model and the mixed-sensitivity H_∞ method used for control design.

4.1 General Model

The method used to synthesize the controller is the S/KS mixed-sensitivity H_∞ method. The standard form of the S/KS mixed-sensitivity optimization is shown in Fig. 4.1, where w is the reference or set-point, z is the error signals, v is the error between reference and output, and u is the voltage signal to helicopter. $z_1 = W_1(r-y)$, $z_2 = W_2u$, and y is the output. K represents the designed controller, G represents the helicopter device, and W_1, W_2 are weighting functions.

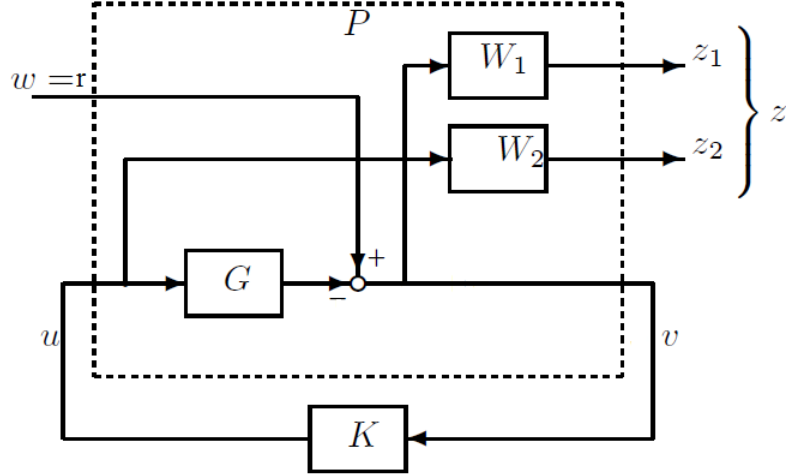


Figure 4.1: S/KS Mixed-sensitivity Minimization in Standard Form [23]

The objective is to find a stabilizing controller that minimizes Eq. (4.1). K represents the controller in the equation $S = (G + K)^{-1}$, and G is the helicopter transfer function. S is the transfer function of the closed-loop matrix from the reference w to the tracking error v , and KS is the transfer function between the reference w to the control signals u .

$$\left\| \begin{bmatrix} W_1 S \\ W_2 K S \end{bmatrix} \right\|_{\infty} \quad (4.1)$$

In this control-education experiment our system is a MIMO system, therefore the weighting functions W_1 and W_2 are matrices. In addition, the weighting functions are defined as diagonal matrices. Every diagonal element weights the respective error from the reference set-point of the transfer function. The close-loop system is a 3 input, 3 output system, and the controller is a 3 input, 2 output system. The

weighting functions W_1 and W_2 can be written as in Eqs. (4.2).

$$W_1 = \begin{bmatrix} W_{11} & 0 & 0 \\ 0 & W_{12} & 0 \\ 0 & 0 & W_{13} \end{bmatrix} \quad W_2 = \begin{bmatrix} W_{21} & 0 \\ 0 & W_{22} \end{bmatrix} \quad (4.2)$$

In general, the W_{1i} and W_{2i} are written as first-order transfer functions because it is simple and effective. The standard form for the elements in the W_1 and W_2 can be written as $\frac{s/M+\omega_B}{s+\omega_B A}$. In this control-education experiment we also select first-order transfer functions as weighting functions. We rewrite it as $a_i \frac{s+b_i}{s+c_i}$ because this form is simple. b_i and c_i represent zeros and poles in the weighting functions. The gain at higher frequencies and lower frequencies can be easily observed in this form.

The program to synthesize the controller is ‘hinfyn’ in MATLAB, which generates the H_∞ optimal controller for the linear time-invariant (LTI) plant. First, the weighting functions are combined with the model of the helicopter, and the general control configuration is shown in Fig. 4.2.

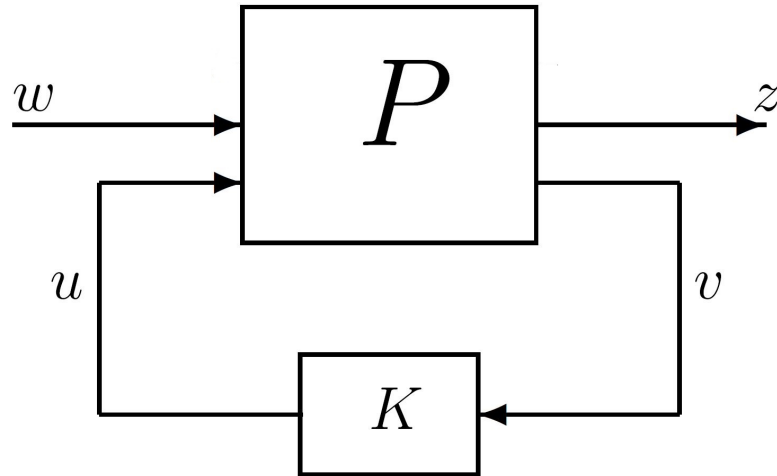


Figure 4.2: General Control Configuration [23]

It is not difficult to show that the generalized plant P is

$$\begin{aligned} P_{11} &= \begin{bmatrix} W_1 \\ 0 \end{bmatrix} & P_{12} &= \begin{bmatrix} -W_1 G \\ -W_2 \end{bmatrix}, \\ P_{21} &= I & P_{22} &= -G \end{aligned} \tag{4.3}$$

where the partitioning is such that:

$$\begin{bmatrix} z_1 \\ z_2 \\ v \end{bmatrix} = \begin{bmatrix} P_{11} & P_{12} \\ P_{21} & P_{22} \end{bmatrix} \begin{bmatrix} w \\ u \end{bmatrix}.$$

Second, apply the ‘hinfyn’ function to the generalized plant P . It determines a (sub)optimal H_∞ control law based on the prescribed open-loop interconnection. The default method is a standard 2-Riccati method [24]. The controller is returned in state-space form, therefore the simulation based on the discrete-time finite difference method can be calculated.

4.2 Selecting Weighting Functions

Selecting weighting functions is very important in the H_∞ control design process because it directly influences the results. Although there are some simple rules for the selection of the weighting functions during the control design, the process is quite subjective.

As mentioned before, $S(s) = (I + GK)^{-1}$ is the transfer function of the closed-loop matrix from the reference w to the tracking error v . For good tracking accuracy in each of the integral outputs the sensitivity function is required to be small. In tuning W_1 it is found that a finite attenuation at high frequencies is useful in reducing

overshoot. Therefore, the gain of the weighting function W_1 should be larger at lower frequencies. KS is the transfer function between the reference w to the control signals u . By limiting the input magnitudes at high-frequencies, the closed-loop bandwidth can be limited. The low-frequency gain of W_2 should be small to ensure that the cost function Eq. (4.1) is dominated by W_1 at low frequencies. The high-frequency gain of W_2 can be increased to limit fast actuator movement. In other words, W_1 are high-gain low-pass filters and W_2 are high-pass filters.

Chapter 5

Software Structure

In general, there are five steps in control design:

1. Analysis of the problem
2. Modeling of the plant and determination of parameters
3. Design of controller
4. Simulation testing and performance assessment
5. Experimental testing

In this control-education experiment, we can refine these steps and illustrate them in

Fig. 5.1.

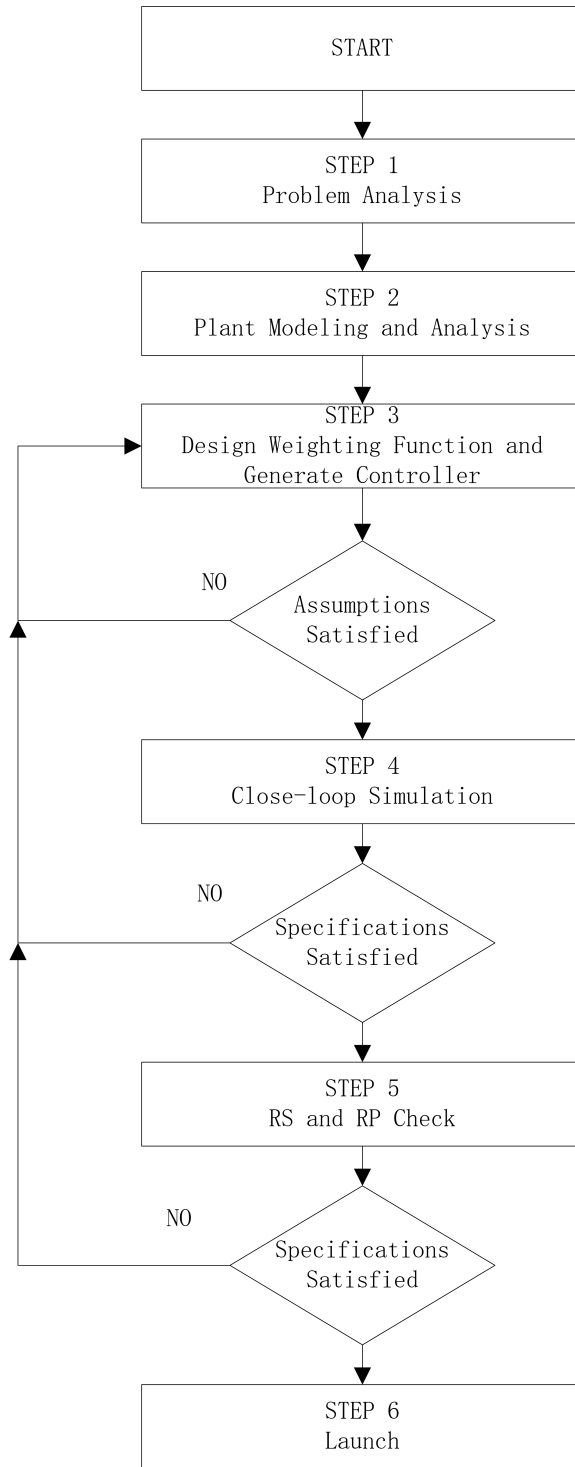


Figure 5.1: Flowchart of the Control-design Process in this GUI

Before designing a controller for a system, it is necessary to have a valid mathematical model of the plant. Since this helicopter system is a highly-coupled and

nonlinear system, it may be difficult for users to model this plant rapidly and properly. In this control-education experiment the mathematical model of the helicopter device is already provided. The approximate values of the physical model parameters are provided too. The main objective for users is to design a robust controller rather than to model the plant. Consequently, the first and the second steps in the robust-control design have been carried out in advance.

For user-friendliness, we designed a GUI using the related functions in Matlab. The GUI module in Matlab provides point-and-click control of software applications, eliminating the need to learn a language or type commands in order to run the application. By utilizing the GUI module, students can save time in programming. Matlab provides widgets such as Button, Edit Text, Static Text, and Axes. In this thesis work, the GUI screen is composed by the following windows:

1. Initial Condition and Set-point Window
2. Weighting Functions Window
3. Model Adjustment Window
4. Assumptions Check Window
5. Simulation Window
6. Experimental Results Window
7. Robust Stability and Performance Window

The GUI screen also has several buttons for users to operate as shown in Fig. 5.2. In the GUI screen, the controller can be synthesized based on the inputs from users. The set points or references can also be specified. The real-time pose is measured by encoders and loaded into the GUI by the DAQ. The error between the set points

and the real-time pose are inputted into the controller. Then, the controller sends voltage signals to the mathematical model in the GUI or the DAQ in order to analyze closed-loop performance either in simulations or in experimental tests as shown in Fig. 5.3.

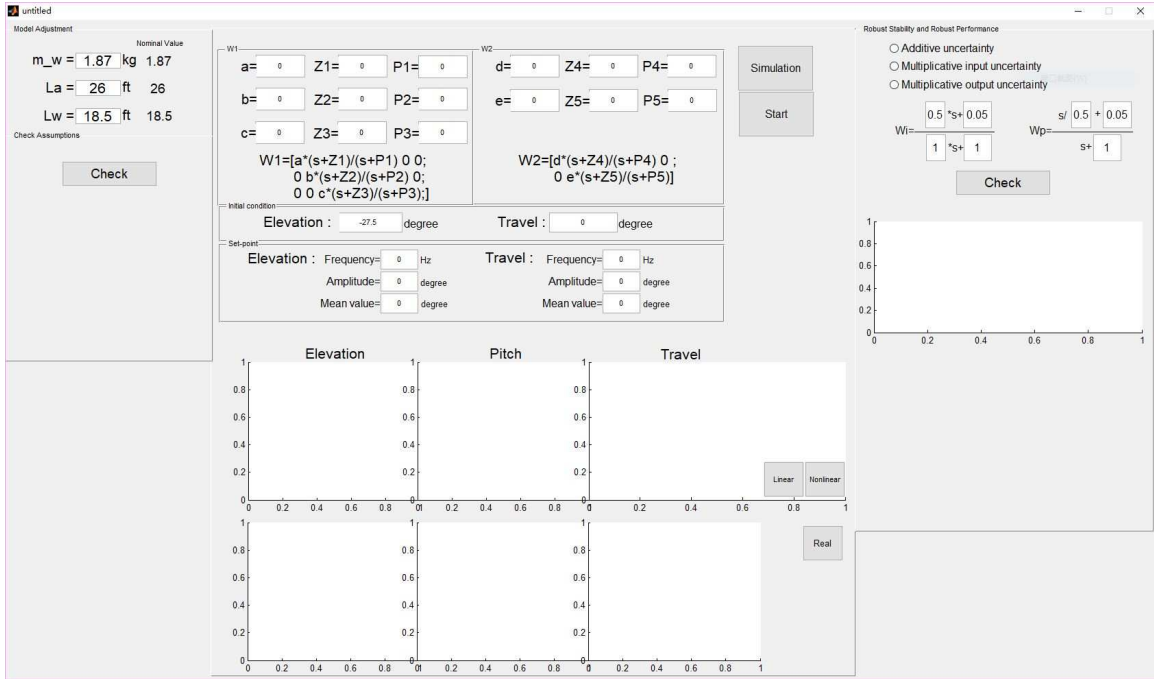


Figure 5.2: Appearance of the GUI

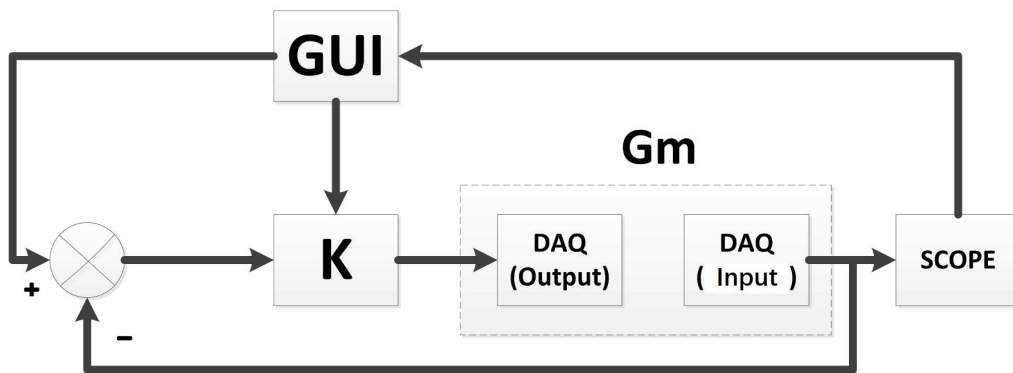


Figure 5.3: Structure of Software

5.1 Initial Condition and Set-point Window

In the initial condition and set-point window, as shown in Fig. 5.4, users can adjust the initial condition of the elevation, pitch and travel angles in simulation. Considering the real helicopter device is placed on a table, the initial elevation angle is approximately -27.5 degrees. Therefore, the default initial condition of the elevation angle is -27.5 degrees.

Users can also adjust the set-point angle of elevation and travel in this window for simulation. The pitch angle is controlled to zero at all times. The set-point of the elevation and travel angles can be set as a square wave with three options: frequency, mean value, and amplitude. The maximum value of a wave signal is equal to the mean value plus the amplitude. Since this system is highly-coupled and nonlinear, we assume that the equilibrium point is zero when linearizing the system dynamics. The maximum value or the mean value of the elevation angle is suggested to be zero. The set-point of the travel angle should not be set as zero in the simulation. The real helicopter device cannot maintain travel angle at zero at the beginning because of uncertainty and disturbance. During the experiment, we recommend users to raise the set-point of the travel angle from thirty to fifty.

Initial condition	
Elevation :	-27.5 degree
Travel :	0 degree

Setpoint	
Elevation :	Frequency= 0 Hz
	Amplitude= 0 degree
	Mean value= 0 degree
Travel :	Frequency= 0 Hz
	Amplitude= 0 degree
	Mean value= 0 degree

Figure 5.4: Appearance of the Initial Condition and Set-point Window

5.2 Weighting Functions Window

In the weighting functions window, users can adjust the parameters of weighting functions. As explained in section 4.1, Z_i represent zeros for each $i = 1, \dots, 5$ and P_i represent poles for each $i = 1, \dots, 5$. The parameters a , b , c , d , and e are the gains at high-frequencies. For example, $a * (s + Z1)/(s + P1)$ is W_{11} in Eqs. (4.2). The appearance of the weighting function window is shown in Fig. 5.5

The image shows a software window titled 'Weighting Functions Window' divided into two panels, W1 and W2. Each panel contains three rows of input fields for parameters and their corresponding transfer function matrices.

Panel W1:

- Row 1: $a = 0$, $Z1 = 0$, $P1 = 0$
- Row 2: $b = 0$, $Z2 = 0$, $P2 = 0$
- Row 3: $c = 0$, $Z3 = 0$, $P3 = 0$

Transfer function matrix for W1:

$$W1 = \begin{bmatrix} a*(s+Z1)/(s+P1) & 0 & 0 \\ 0 & b*(s+Z2)/(s+P2) & 0 \\ 0 & 0 & c*(s+Z3)/(s+P3) \end{bmatrix}$$

Panel W2:

- Row 1: $d = 0$, $Z4 = 0$, $P4 = 0$
- Row 2: $e = 0$, $Z5 = 0$, $P5 = 0$

Transfer function matrix for W2:

$$W2 = \begin{bmatrix} d*(s+Z4)/(s+P4) & 0 \\ 0 & e*(s+Z5)/(s+P5) \end{bmatrix}$$

Figure 5.5: Appearance of the Weighting Functions Window

5.3 Model Adjustment Window

Although the actual helicopter device and the mathematical model provided by Quanser definitely have differences, those differences are subtle. On the other hand, the helicopter device is hard to change. Dismounting and assembling the helicopter in order to change the parameters is time-consuming. Since our goal is to design a device for educational purposes, this apparatus should be convenient to use. Students should not consume significant time on assembly and disassembly. Therefore, we designed a model adjustment window as shown in Fig. 5.6, which allows students to change some parameters of the mathematical model with the purpose of magnifying the differences between the model and the actual system. Among all the parameters in state space equations, some parameters cannot be adjusted, such as the propeller

force-thrust constant and motor current-torque constant. Some parameters' adjustments are not obvious, such as the distance between the pitch pivot and each motor. Therefore, in this control-education experiment, we selected three parameters which users can adjust: the mass of counter-weight (m_w), the distance between elevation pivot to helicopter body (L_a) and the distance between elevation pivot to counter-weight (L_w). Users can adjust these parameters at the same time or individually in order to represent the parametric uncertainty. In this GUI, Matlab can synthesize a robust controller with the 'hinsyn' function based on the length or weight parameters entered by users, and then plot the close-loop dynamic response of three angles in two ways: the first one is based on the model, which is modified by users, and the second one is based on the precise model provided by Quanser. The first one is represented by green line and the second one is represented by red line in the simulation result. The appearance of the model adjustment window is shown in Fig. 5.6 and the values in this figure are the nominal values.

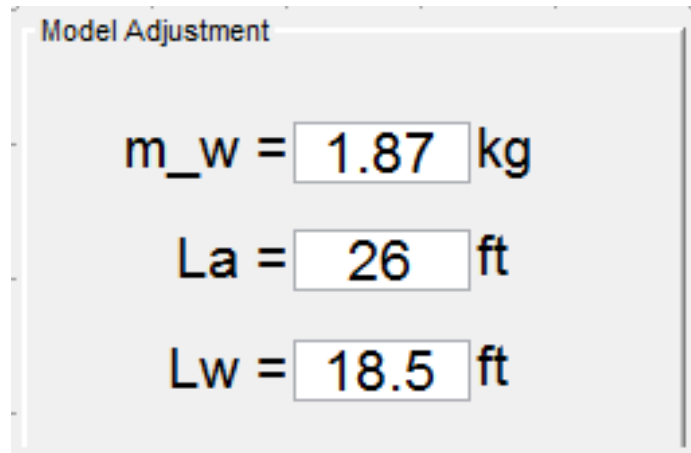


Figure 5.6: Appearance of the Model Adjustment Window

5.4 Assumptions Check Window

Recalling that the generalized plant P in Eqs. (4.3). The state-space matrices of P can be obtained by converting the transfer functions Eqs. (4.3) to the state-space form in MATLAB. The state-space of P is

$$P = \begin{bmatrix} A & B \\ C & D \end{bmatrix}, \quad (5.1)$$

where A is a 11×11 matrix and D is a 8×5 matrix. Rewrite Eq. 5.1 as

$$P = \begin{bmatrix} A & B_1 & B_2 \\ C_1 & D_{11} & D_{12} \\ C_2 & D_{21} & D_{22} \end{bmatrix},$$

where inputs to B_2 are the control inputs, and outputs of C_2 are the output measurements provided to the controller. Therefore, B_2 is a 11×2 matrix and C_2 is a 3×11 matrix.

In the H_∞ problem, some assumptions are typically made in order to solve such problem. Among all assumptions, two assumptions are the most important. The first one is that (A, B_2, C_2) is stabilizable and detectable and the second one is that D_{12} and D_{21} have full rank. The first assumption is required for the existence of a stabilizing controller K , and the second assumption is sufficient to ensure the controllers are proper and hence realizable. Because of this, we designed a window in the GUI for users to check these two assumptions before they start synthesizing a controller. The method is to calculate the eigenvalues of matrix A first and then to apply the Popov-Belevitch-Hautus test to every eigenvalue. The next step is to check whether all unobservable or uncontrollable modes are stable. If so, that means the matrix

(A, B_2, C_2) is stabilizable and detectable. It is much easier to test whether D_{12} and D_{21} have full rank or not. The appearance of the assumptions check window is shown in Fig. 5.7.

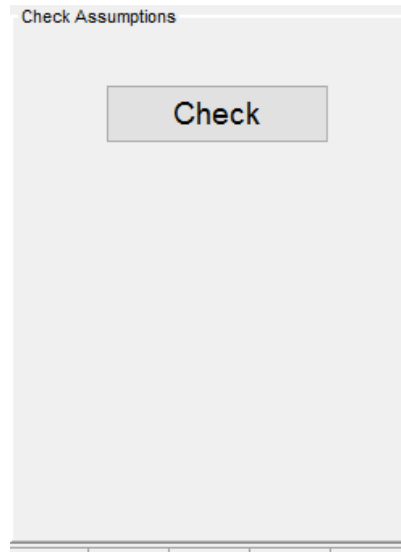


Figure 5.7: Appearance of the Assumptions Check Window

5.5 Simulation Window

After clicking on the “Simulation” button, the user’s input is loaded, and the linear or nonlinear simulation results for these three angles are returned. There are two buttons to determine which one is plotted. The appearance of the simulation window is shown in Fig. 5.8.

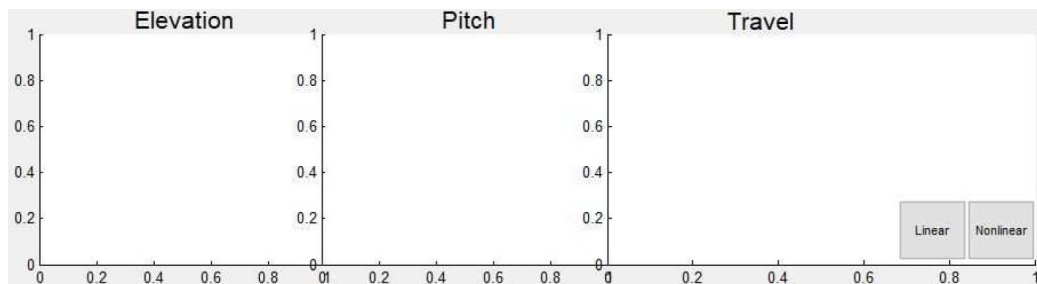


Figure 5.8: Appearance of the Simulation Window

The simulation results are calculated by the finite difference method. Since the state-space models of the controller and the helicopter are known, we can calculate the outputs of these two blocks based on the inputs and the state-space matrices.

The discrete equations for the controllers are shown in Eqs. 5.2.

$$\begin{cases} \frac{x_{i+1} - x_i}{\Delta t} = A_K * x_{i+1} + B_K * (r_i - y_i) \\ u_{i+1} = C_K * x_{i+1} \end{cases}. \quad (5.2)$$

This is the implicit expression, and it can be rewritten as:

$$\begin{cases} x_{i+1} = (I - \Delta t * A_K)^{-1} * (x_i + \Delta t * B_K * (r_i - y_i)) \\ u_{i+1} = C_K * x_{i+1} \end{cases},$$

where r_i is the reference or set point, y_i is the output of the helicopter, and Δt is the time step. (A_K , B_K , C_K) are the matrices of controller's state-space model, and u_i is the voltage signal from controller to the rotors. The max value of the voltage signal is limited to 12V because the nominal voltage of the motor we use is 12V. These variables are defined in Eqs. 5.3. ϵ is the elevation angle, ρ is the pitch angle, and λ is the travel angle. V_f is the voltage signal to the front rotor, and V_b is the voltage signal to the back rotor.

$$r_i = \begin{bmatrix} \epsilon_i \\ \rho_i \\ \lambda_i \end{bmatrix}_d \quad y_i = \begin{bmatrix} \epsilon_i \\ \rho_i \\ \lambda_i \end{bmatrix} \quad V_i = \begin{bmatrix} V_f \\ V_b \end{bmatrix}_i \quad (5.3)$$

For the linear simulation, the discrete-time equations for the helicopter model are

shown in Eqs. 5.4.

$$\begin{cases} \frac{x_{i+1} - x_i}{\Delta t} = A_G * x_{i+1} + B_G * u_i \\ y_{i+1} = C_G * x_{i+1} + D_G * u_i \end{cases} \quad (5.4)$$

This is an implicit expression as well and can be rewritten as

$$\begin{cases} x_{i+1} = (I - \Delta t * A_G)^{-1} * (x_i + \Delta t * B_G * u_i) \\ y_{i+1} = C_G * x_{i+1} + D_G * u_i \end{cases},$$

where (A_G, B_G, C_G, D_G) are the matrices of the helicopter's mathematical models in state-space form . They represent Eqs. (3.5) or Eqs. (3.6).

For the nonlinear simulation, the relationship between the input voltages and the position cannot be written as a state-space. Therefore, the relationship between the input voltages and the position can be written as the nonlinear model Eqs. (3.2) in section 3.2. The discrete-time acceleration can then be calculated. The angular velocity and the angle can be derived as well.

$$\begin{bmatrix} \dot{\epsilon} \\ \dot{\rho} \\ \dot{\lambda} \end{bmatrix}_i = \begin{bmatrix} \dot{\epsilon} \\ \dot{\rho} \\ \dot{\lambda} \end{bmatrix}_{i-1} + \begin{bmatrix} \ddot{\epsilon} \\ \ddot{\rho} \\ \ddot{\lambda} \end{bmatrix}_i \Delta t \quad \begin{bmatrix} \epsilon \\ \rho \\ \lambda \end{bmatrix}_i = \begin{bmatrix} \epsilon \\ \rho \\ \lambda \end{bmatrix}_{i-1} + \begin{bmatrix} \dot{\epsilon} \\ \dot{\rho} \\ \dot{\lambda} \end{bmatrix}_i \Delta t$$

In this control-education experiment, the time step is 0.01 seconds, and the number of steps is six thousand. Since we use the implicit method, it returns meaningful results.

5.6 Experimental Results Window

When users confirm that the system is stable under these weighting functions, they can utilize the “Start” button, as shown in Fig. 5.2, to load the controller into the workspace, implement the controller, activate the Simulink model, and control the actual helicopter device. When actual helicopter device is stopped by users, all the pose information recorded by the encoders is saved in the workspace of MATLAB. Users can plot the control results in this window by clicking the “Real” button. The appearance of it is shown in Fig. 5.9.

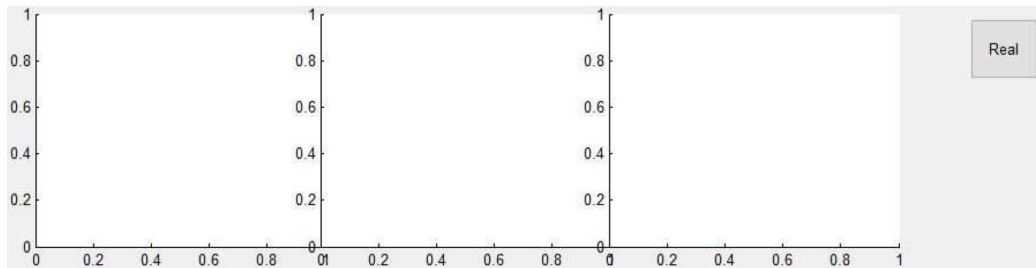


Figure 5.9: Appearance of the Experimental Results Window

5.7 Robust Stability and Performance Window

In the robust stability and performance window, users can assess the robust stability and performance condition by structured singular values. In this control-education experiment, we assume the types of unstructured uncertainty only belong to three different types, multiplicative input uncertainty, multiplicative output uncertainty, and additive uncertainty, because these three types are typical uncertainties that exist in almost every system. For example, the multiplicative input uncertainty can reflect the noise in voltage signals, the errors from amplifying modules, and the disturbance from outside of our devices. Users can select which type of uncertainty they want in Fig. 5.12.

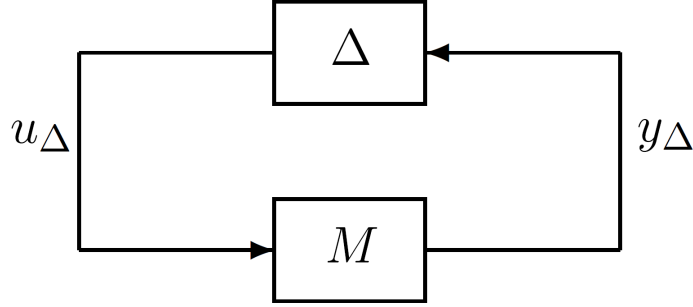


Figure 5.10: $M\Delta$ -Structure for Robust Stability Analysis

Once we assume the type of unstructured uncertainty, the general control configuration can be calculated easily. Then the $M\Delta$ -structure, as shown in Fig. 5.10, can be obtained as well. We use the small-gain theorem

$$RS \longleftrightarrow \mu(M) < 1 \quad \forall \omega,$$

where $\mu(M)$ is the structured singular value of M . The calculation of μ makes use of the fact that Δ has a given block-diagonal structure, where certain blocks may also be real. We defined robust performance (RP) as $\|F_u(N, \Delta)\|_\infty < 1$ for all allowed Δ 's, where N is shown in Fig. 5.11. Since we used the H_∞ norm in both the representation of uncertainty and the definition of performance, we found that RP could be viewed as a special case of RS, and we derived

$$RP \longleftrightarrow \mu(N) < 1 \quad \forall \omega,$$

where μ is computed with respect to the block-diagonal structure $\text{diag}\{\Delta, \Delta_p\}$. Here Δ represents the uncertainty, and Δ_p is a fictitious full uncertainty block representing the H_∞ performance bound.

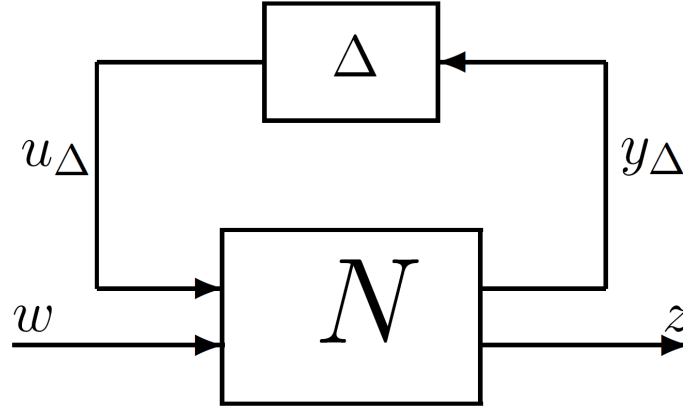


Figure 5.11: $N\Delta$ -Structure for Robust Performance Analysis

In the robust stability and performance window, the W_i represents the weighting function of unstructured uncertainty, such as w_A , w_I and w_O in Fig. 3.2-Fig. 3.4. The default value of W_i in our experiment is $\frac{0.5*s+0.05}{s+1}$. This implies a relative uncertainty of up to 5% in the low-frequency range, which increases at high-frequency range, reaching a value of 50%. The increase in frequency compensates for various neglected dynamics associated with the actuator. The W_i showed in the robust stability and robust performance window is a scalar, but it represents the uncertainty matrix. Depending on the type of uncertainty users choose, this matrix can be written as a 2×2 , 3×3 or 3×2 matrix as follows:

$$W_i * \begin{bmatrix} 1 & 0 \\ 0 & 1 \end{bmatrix} \quad or \quad W_i * \begin{bmatrix} 1 & 0 & 0 \\ 0 & 1 & 0 \\ 0 & 0 & 1 \end{bmatrix} \quad or \quad W_i * \begin{bmatrix} 1 & 0 \\ 0 & 1 \\ 0 & 0 \end{bmatrix}$$

W_p are the weighting functions of performance, which is defined as the pose of the helicopter. The default value of W_p is $\frac{s/0.5+0.05}{s+1}$. Consequently, the weighting function W_p is a 3×3 diagonal matrix. The three weighting functions in the diagonal are the corresponding angles. Although the weighting functions of corresponding angles can

be different, it can be simplified by assuming the weighting functions of three angles are the same. Thus, similar to the weighting functions of uncertainty, W_p is defined as in Eq. 5.5 for three different types of uncertainty.

$$W_p * \begin{bmatrix} 1 & 0 & 0 \\ 0 & 1 & 0 \\ 0 & 0 & 1 \end{bmatrix} \quad (5.5)$$

Users can also adjust the parameters of W_i and W_p in order to understand the meaning of weighting functions of uncertainty. When users click on the check button, the curves, which represent robust stability and robust performance, will be plotted. The appearance of the robust stability and performance window is shown in Fig. 5.12.

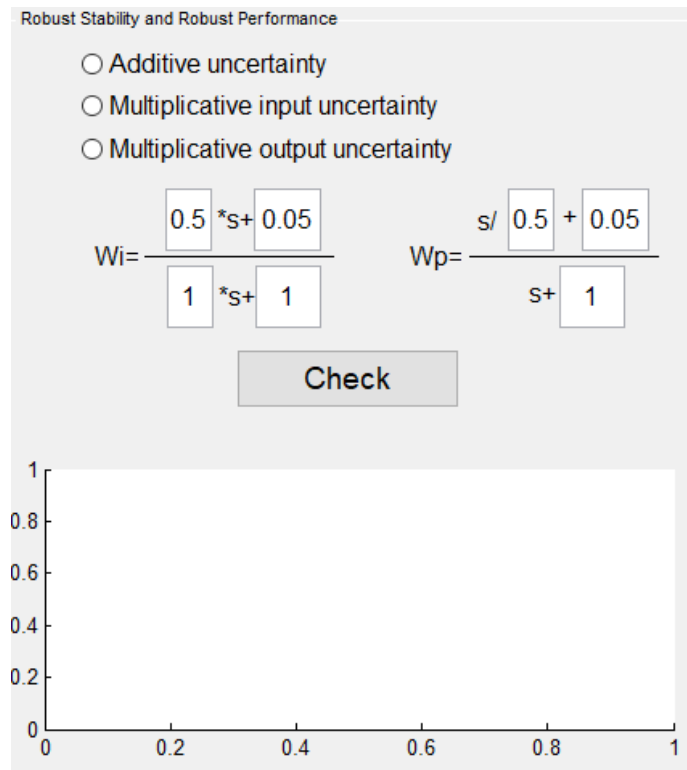


Figure 5.12: Appearance of the Robust Stability and Performance Window

Chapter 6

Experimental Demonstrations

In order to demonstrate this robust control education system, we tested several controllers synthesized on our GUI. Some pre-lab work should be done before using the GUI, such as getting the mathematical model of the helicopter and analyzing the position of poles and zeros. Since the weighting functions may forge the close-loop system as the user's requirements, we always require the system to have good-tracking and disturbance rejection. Selecting weighting functions should follow the rules mentioned in section 4.2.

6.1 Stabilizing the Nominal Plant

First, we select two weighting functions as shown in the first group below:

$$\text{First group: } W_1 = \begin{bmatrix} 5 * \frac{s+7}{s+0.5} & 0 & 0 \\ 0 & 5.5 * \frac{s+7}{s+0.5} & 0 \\ 0 & 0 & 5 * \frac{s+7}{s+0.5} \end{bmatrix} \text{ and}$$

$$W_2 = \begin{bmatrix} 0.5 * \frac{s+1}{s+10} & 0 \\ 0 & 0.5 * \frac{s+1}{s+10} \end{bmatrix}.$$

In the assumption check window, after clicking on the “Check” button, the GUI shows that “(A, B2, C2) is stabilizable and detectable” and “D12 and D21 have full rank” as in Fig. 6.1, which means this generalized plant satisfies the assumptions.

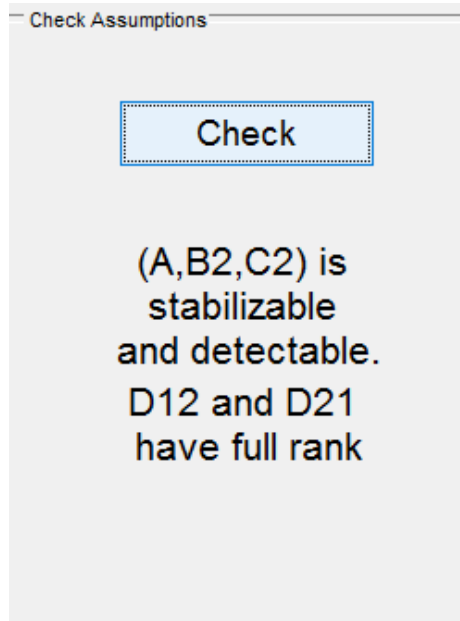


Figure 6.1: Demo of the Assumptions Check Window

The initial conditions and set-points are configured as in Fig. 6.2. The reasons were explained in section 5.1.

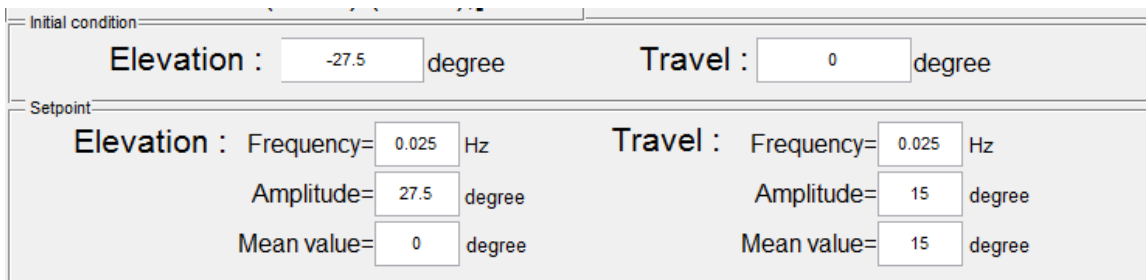


Figure 6.2: Demo of the Initial Conditions and the Set-points

The simulated dynamic response of the control system is plotted on the monitor automatically when users click on the “Simulation” button. The linear and nonlinear simulation results are shown in Fig. 6.3 and Fig. 6.4.

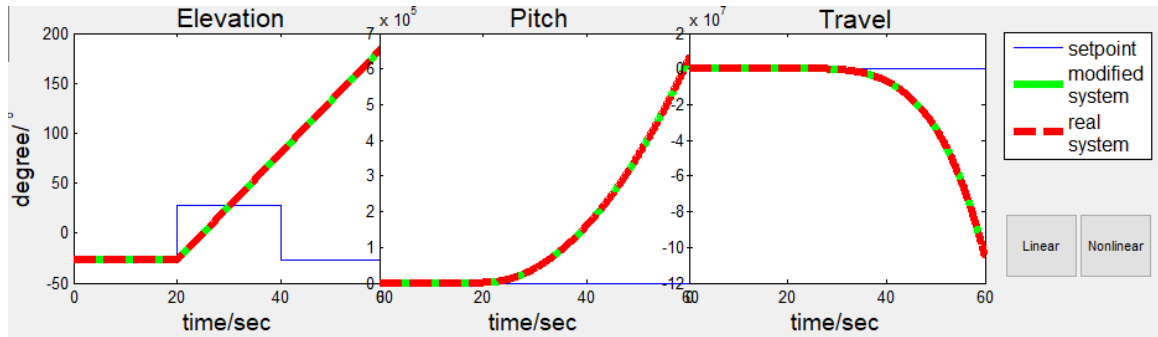


Figure 6.3: Linear Dynamic Response Simulation of the First Group

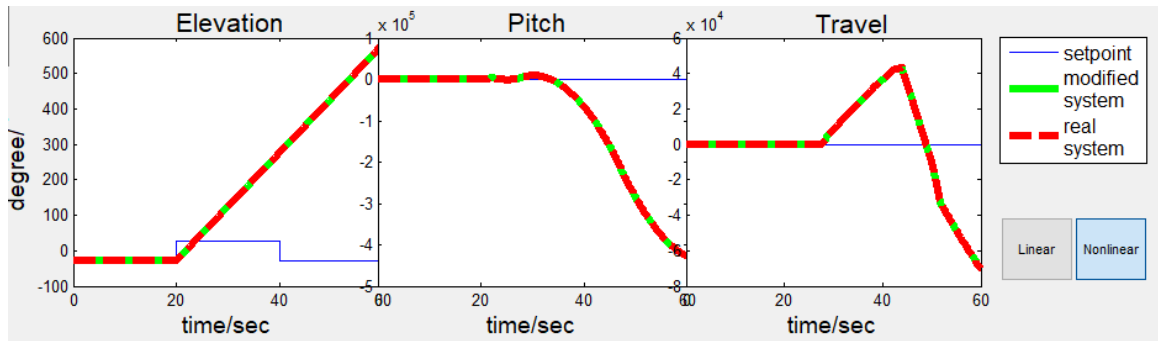


Figure 6.4: Nonlinear Dynamic Response Simulation of the First Group

Apparently, this close-loop system is unstable, because the gain for W_1 and W_2 at lower frequencies is too small. When adjustments are made, the second group weighting functions are:

$$\text{Second group: } W_1 = \begin{bmatrix} 10 * \frac{s+100}{s+0.01} & 0 & 0 \\ 0 & 30 * \frac{s+100}{s+0.01} & 0 \\ 0 & 0 & 0.1 * \frac{s+100}{s+0.01} \end{bmatrix} \text{ and}$$

$$W_2 = \begin{bmatrix} 200 * \frac{s+0.001}{s+10} & 0 \\ 0 & 200 * \frac{s+0.001}{s+10} \end{bmatrix}.$$

W_1 is a low-pass filter and W_2 is a high-pass filter, which satisfies the requirement in section 4.2. In this example, the poles and zeros are the same in each matrix entry. It is not necessary in this form, but it is already sufficient to produce proper controllers. The parameters of the weighting functions can be changed easily in the weighting functions window. The linear and nonlinear simulations are shown in Fig. 6.5 and Fig. 6.6. From the graphs, users can confirm stability.

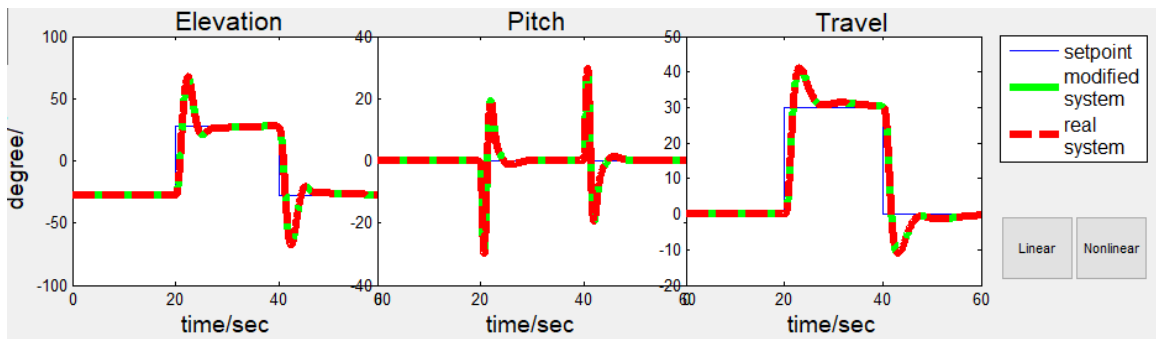


Figure 6.5: Linear Dynamic Response Simulation of the Second Group

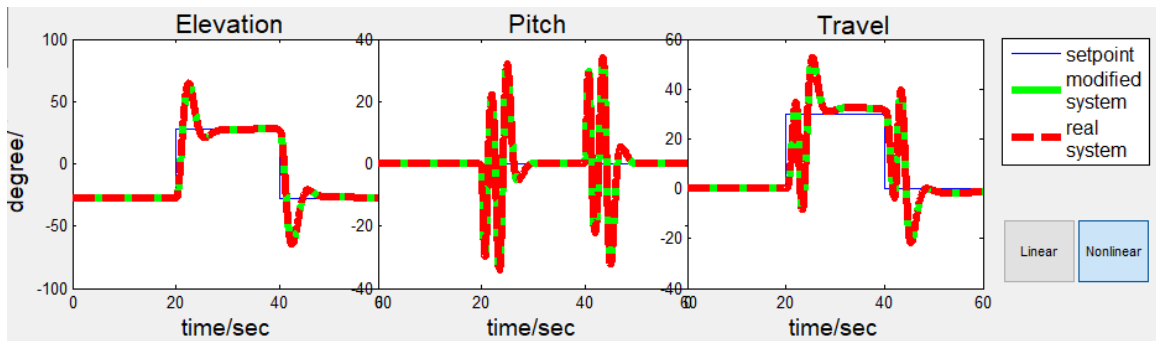


Figure 6.6: Nonlinear Dynamic Response Simulation of the Second Group

6.2 Adjusting Mathematical Model

In the model modification window, users can adjust three parameters of this system. These represent the parametric uncertainty. Although the uncertainty should be a range, the difference between the precise parameters and the modified parameters can be considered as the worst case.

Taking the distance between elevation pivot to helicopter body (L_a) as an example, we adjust L_a from 26 ft to 25 ft and use the second controller designed in the last section for stabilizing the nominal plant. The linear and nonlinear simulation results are shown in Fig. 6.7-6.8.

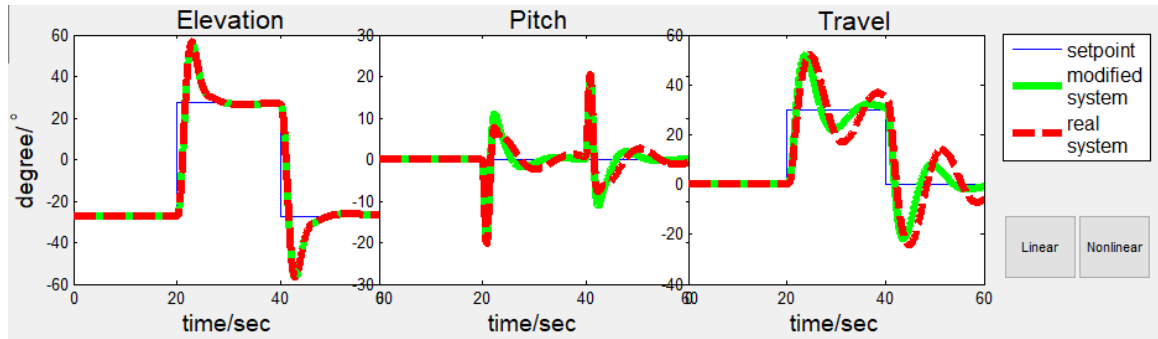


Figure 6.7: Linear Dynamic Response Simulation of the Second Group with $L_a = 25$

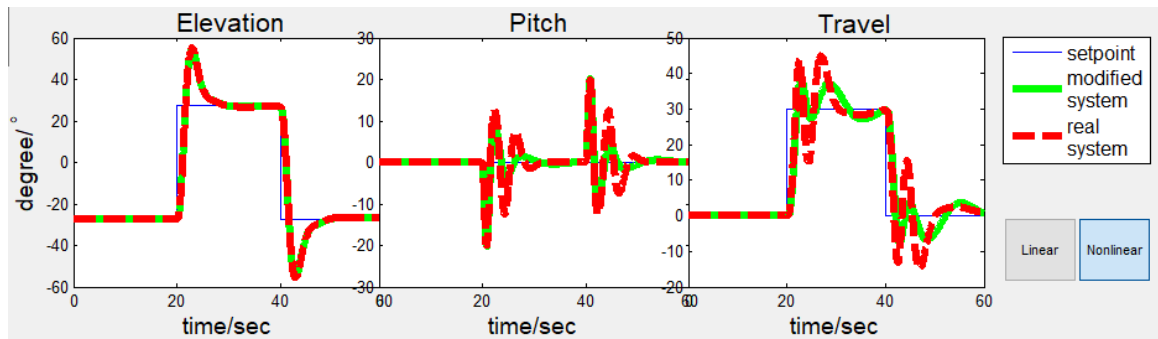


Figure 6.8: Nonlinear Dynamic Response Simulation of the Second Group with $L_a = 25$

In these figures, the red line represents the simulation results based on the precise

model and the green line represents the simulation results based on the modified model. From these figures, we can identify that the dynamic response of the green line is better than that of the red line, and both of them are stable, which means that the controller based on the modified parameters can control both the modified model and the precise model.

If we keep enlarging the range of uncertainty by decreasing the L_a from 25 ft to 23 ft and generate the simulation results as well, we can get the results as shown in Fig. 6.9 and Fig. 6.10.

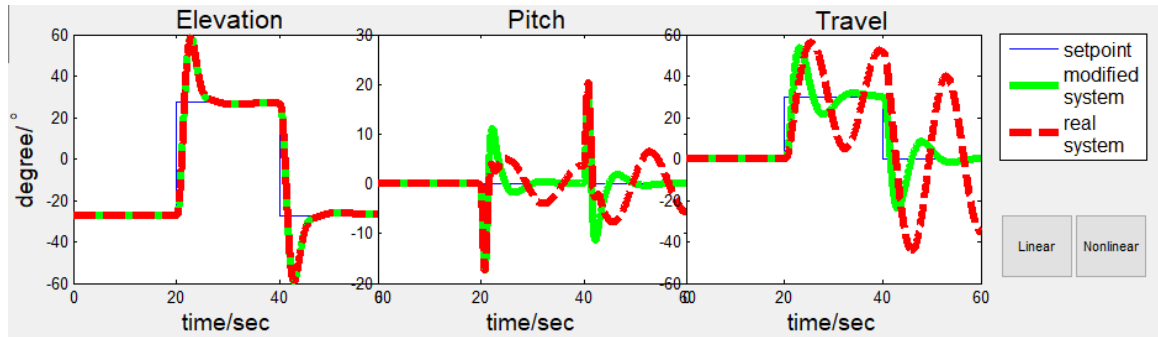


Figure 6.9: Linear Dynamic Response Simulation of the Second Group with $L_a = 23$

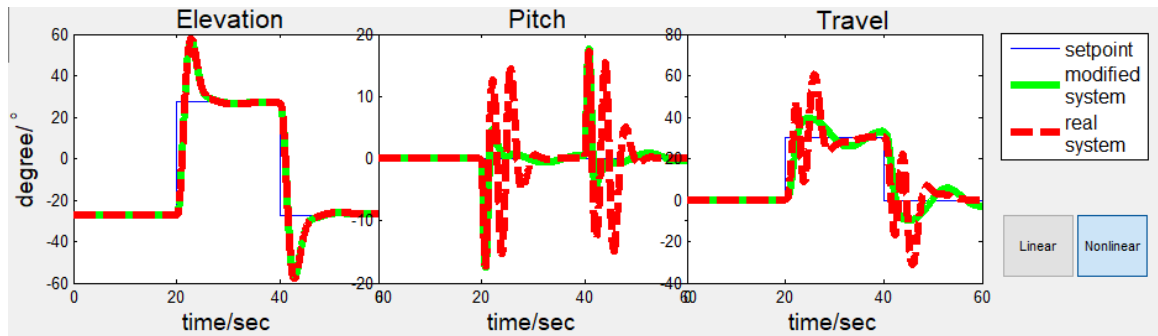


Figure 6.10: Nonlinear Dynamic Response Simulation of the Second Group with $L_a = 23$

These results indicate that the controller design based on the modified parameter can control the modified model with difficulties, and the linear simulation of the

system with ‘uncertainty’ is not good.

In order to control both these systems, we need to select new weighting functions. The third group of weighting functions are shown below.

$$\text{Third group: } W_1 = \begin{bmatrix} 10 * \frac{s+100}{s+0.01} & 0 & 0 \\ 0 & 30 * \frac{s+100}{s+0.01} & 0 \\ 0 & 0 & 0.1 * \frac{s+100}{s+0.01} \end{bmatrix} \text{ and}$$

$$W_2 = \begin{bmatrix} 250 * \frac{s+0.001}{s+20} & 0 \\ 0 & 250 * \frac{s+0.001}{s+20} \end{bmatrix}.$$

We also generated controllers based on these weighting functions and got the simulation results, as shown in Fig. 6.11 and Fig. 6.12.

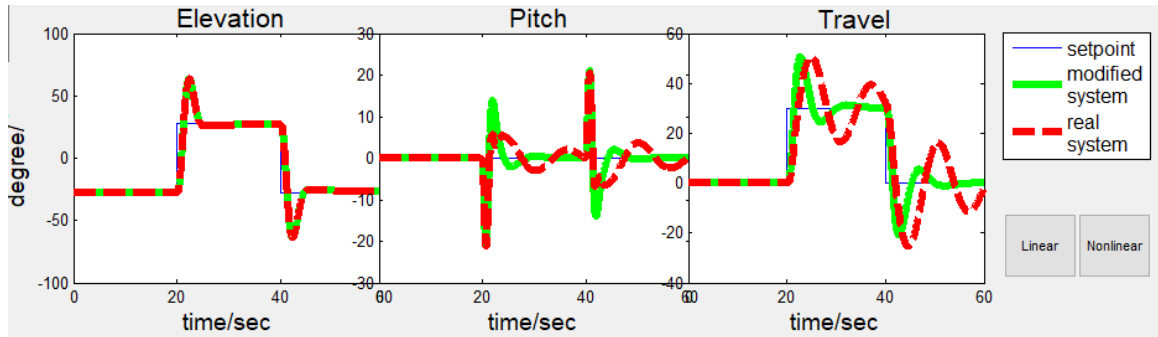


Figure 6.11: Linear Dynamic Response Simulation of the Third Group with $L_a = 23$

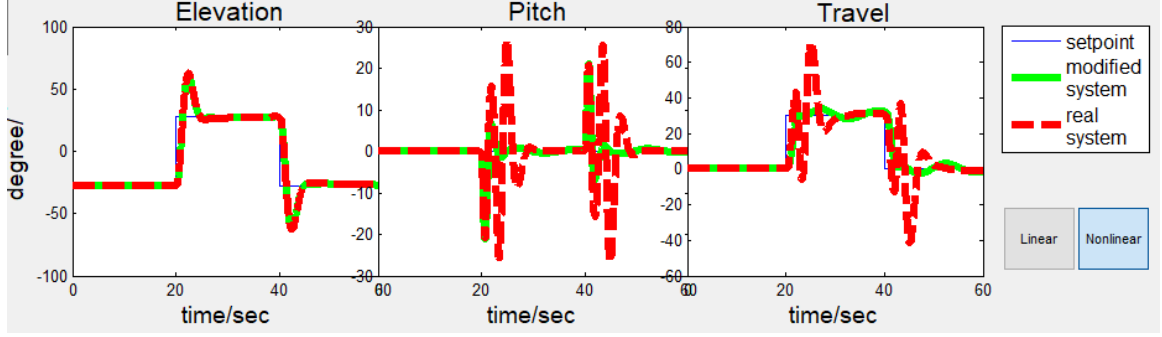


Figure 6.12: Nonlinear Dynamic Response Simulation of the Third group with $L_a = 23$

This result indicates that the controller, based on $L_a = 23$ ft, can control both the modified model and the real system with ‘uncertainty’. It also means that this controller can tolerate approximately 9% uncertainty for L_a .

Users can handle the other two parameters (m_w and L_w) in this way as well. Users can also change more than one parameter simultaneously.

6.3 Assessing Robust Stability and Performance

In this section, the objective is to design a controller that can satisfy robust stability and robust performance. In order to simplify this process, we assume that the parametric uncertainty is negligible and focus on the unstructured uncertainty.

First, we assume that the weighting function of uncertainty is default ($W_i = \frac{0.5*s+0.05}{s+1}, W_p = \frac{s/0.5+0.05}{s+1}$) and select the fourth group weighting functions shown below:

$$\text{fourth group: } W_1 = \begin{bmatrix} 200 * \frac{s+100}{s+0.01} & 0 & 0 \\ 0 & 200 * \frac{s+100}{s+0.01} & 0 \\ 0 & 0 & 10 * \frac{s+100}{s+0.01} \end{bmatrix} \text{ and}$$

$$W_2 = \begin{bmatrix} 500 * \frac{s+0.1}{s+10} & 0 \\ 0 & 500 * \frac{s+0.1}{s+10} \end{bmatrix}.$$

The simulation results are shown in Fig. 6.13 and Fig. 6.14.

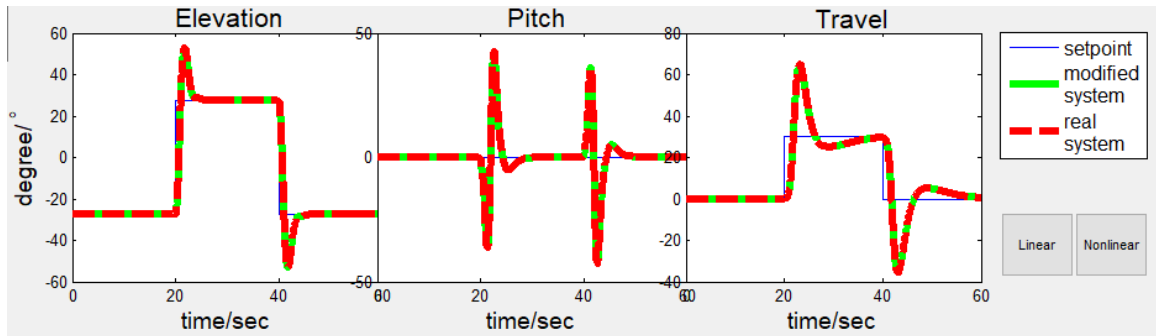


Figure 6.13: Linear Dynamic Response Simulation of the Fourth Group

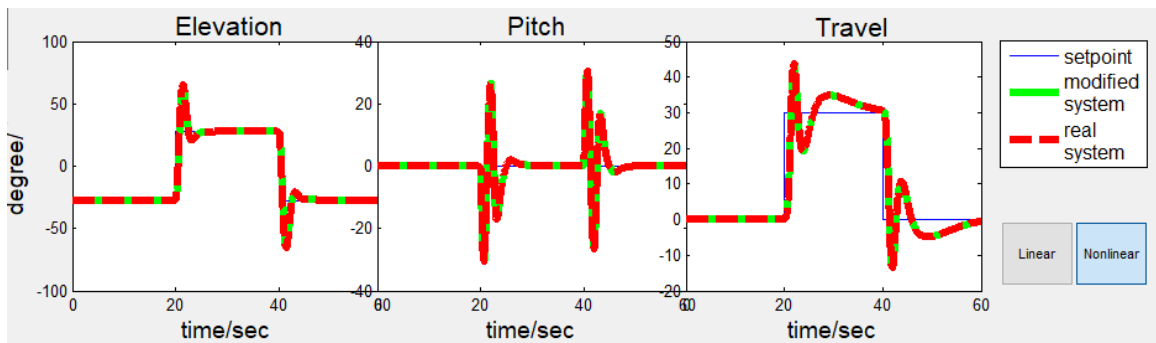


Figure 6.14: Nonlinear Dynamic Response Simulation of the Fourth Group

The multiplicative input uncertainty type is selected. After clicking on the “Check” button in the RS and RP window, the results of μ analysis are shown in Fig. 6.15.

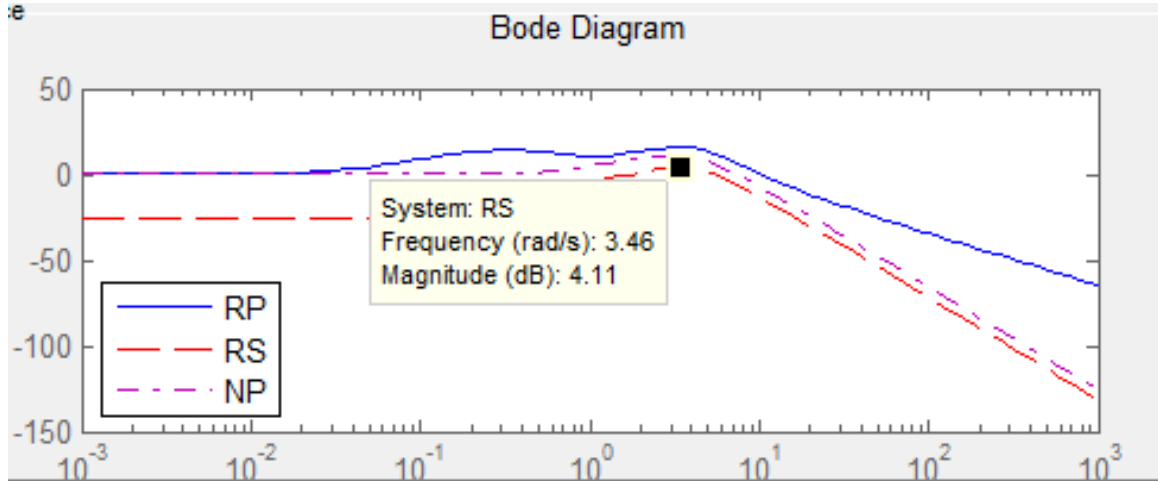


Figure 6.15: μ -analysis Results of the Fourth Group

The maximum value of μ in the bode plot is greater than zero, which means the $\mu(M) > 1$ and the closed-loop system does not satisfy robust stability. Therefore, we must design new weighting functions, as the fifth group shows below:

$$\text{Fifth group: } W_1 = \begin{bmatrix} 20 * \frac{s+100}{s+0.01} & 0 & 0 \\ 0 & 60 * \frac{s+100}{s+0.01} & 0 \\ 0 & 0 & 0.1 * \frac{s+100}{s+0.01} \end{bmatrix} \text{ and}$$

$$W_2 = \begin{bmatrix} 200 * \frac{s+0.1}{s+10} & 0 \\ 0 & 200 * \frac{s+0.1}{s+10} \end{bmatrix}.$$

The simulation results and the results of μ analysis are shown in Fig. 6.16-Fig. 6.18.

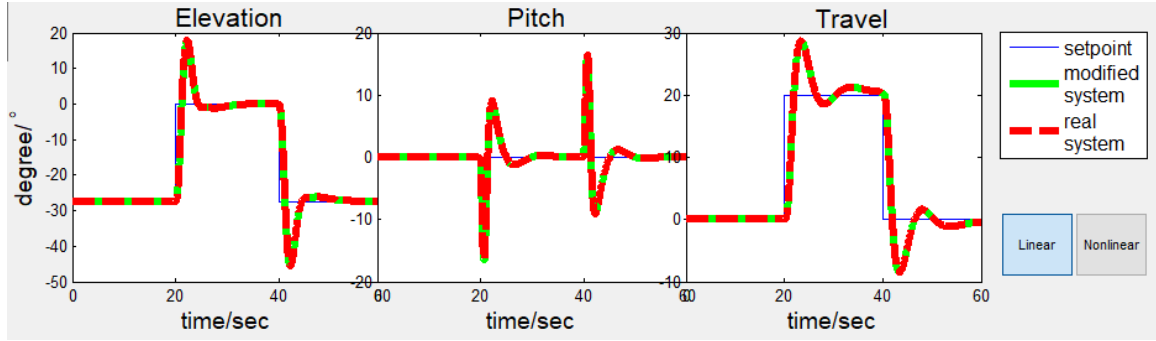


Figure 6.16: Linear Dynamic Response Simulation of the Fifth Group

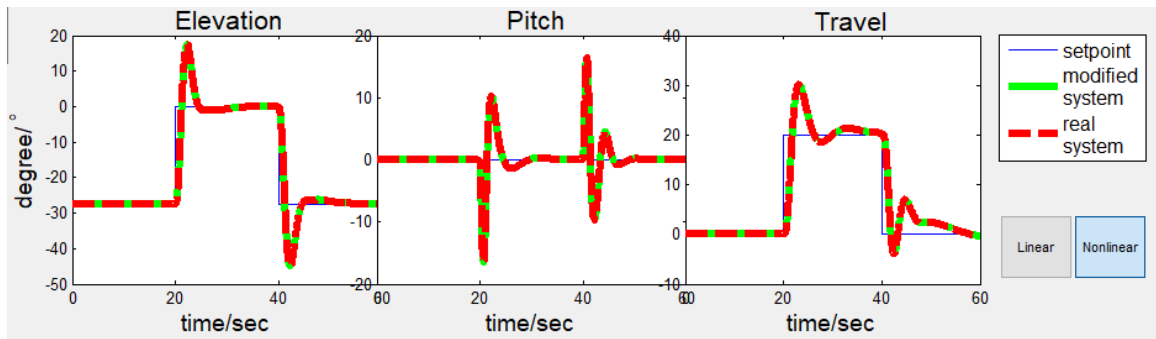


Figure 6.17: Nonlinear Dynamic Response Simulation of the Fifth Group

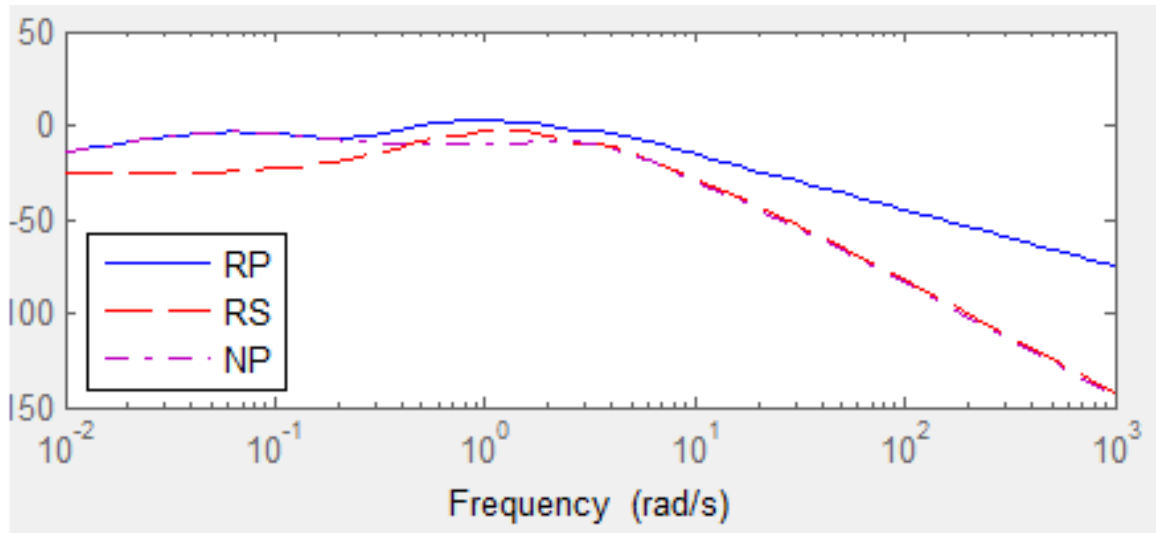


Figure 6.18: μ -analysis Results of the Fifth Group(a)

The maximum value of $\mu(M)$ is smaller than 1, so the robust stability is satisfied

for all frequencies. Meanwhile, under this condition, the RP is higher than 1 for all frequencies, which means that the robust performance is not satisfied for all frequencies. If users adjust the parameters of W_p to $\frac{s/20+0.05}{s+1}$, which means 5% uncertainty at low frequency and 5% uncertainty at high frequency, and then generate the bode plot again, all values are smaller than zero, which means the RS and RP are satisfied for all frequencies. The bode plot is shown in Fig 6.19.

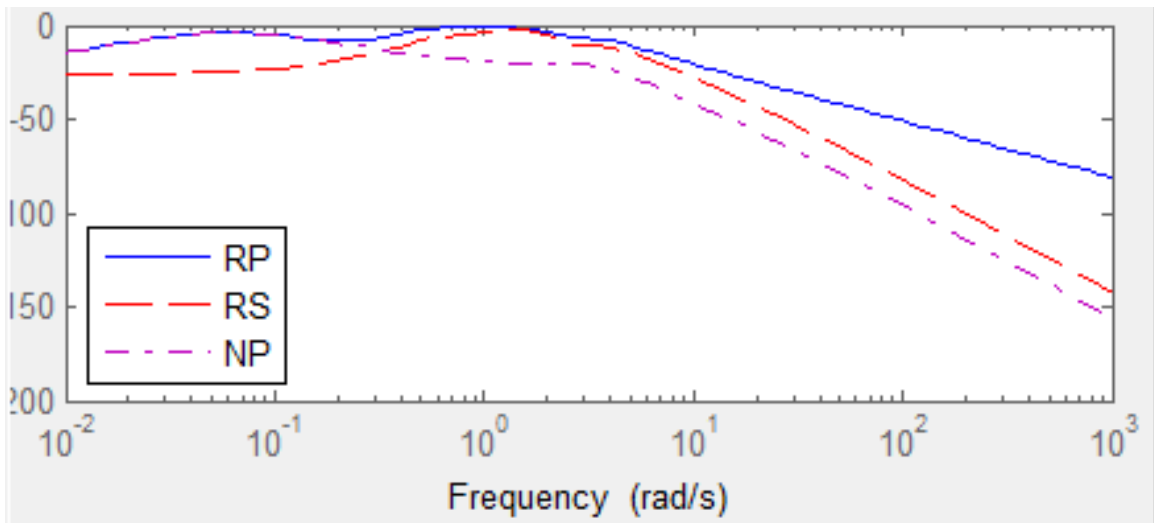


Figure 6.19: μ -analysis Results of the Fifth Group(b)

Users can design a controller to satisfy robust stability and robust performance for specified weighting functions (W_i and W_p) and uncertainty type such as multiplicative output uncertainty and additive uncertainty.

Chapter 7

Conclusion and Future Work

7.1 Conclusion

This contribution presents a user-friendly Graphical Users Interface for students to focus on studying robust-control design rather than debugging the system itself. The system to be controlled is a three degrees of freedom helicopter model, which is analogous to a tandem rotor helicopter, such as the Boeing HC-1B Chinook, commonly used by engineers. This education system minimizes the effort required to program in MATLAB and Simulink for control design, simulation, and analysis. The mathematical model of the helicopter and the uncertainty is briefly described for users to comprehend the control design process. The Graphical User Interface also allows students to change some parameters in the mathematical model and to assess the influence of variant parametric uncertainty easily and quickly without adjusting the real device. The H_∞ mixed-sensitivity method is implemented to synthesize the controller. Unstructured singular values are computed to assess robust stability and robust performance. The unstructured uncertainty is modeled in the frequency domain by assuming weighting functions. Users can also modify the weighting func-

tions of uncertainty and performance to simulate different environments and different requirements for performance.

7.2 Future Work

The method to synthesize controllers and the types of uncertainty are limited. So far, users can only use the S/KS mixed-sensitivity method to synthesize the controller. The available types of uncertainty are limited to three types, and the weighting functions of uncertainty and performance are equal to a scalar times an identity matrix. For future work, other methods to generate controllers should be included. Users could then select the method on their own. The types of uncertainty can be extended to six different types, and the weighting functions of uncertainty and performance can be made more complex.

Bibliography

- [1] Astrom, K. J., and Wittenmark, B., *Adaptive Control Reading*, MA: Addison-Wesley, 1989.
- [2] Landau, I.D., *Adaptive Control: The Model Reference Approach*, Marcel Dekker Inc., 1979.
- [3] Gutman, S. and Palmor, Z., “Properties of min max controller in uncertain dynamic system,” *SIAM J. Control and Optimization*, 1982, 20(2):850-861.
- [4] Corless, M. and Leitmann, G., *Deterministic control of uncertain systems*, London, Peter Peregrinus Ltd, 1990, pp. 220-251.
- [5] Leitmann, G., “Guaranteed asymptotic stability for a class of uncertain linear dynamical systems,” *Journal of Optimization Theory and Applications*, v27, n 1, January 1979, pp. 99-106.
- [6] Leitmann, G. “Guaranteed asymptotic stability for some linear systems with bounded uncertainties,” *Transaction of the ASME*, v101, n 1, September 1979, pp. 212-216.
- [7] Dorato, P. et al., “Bibliography on robust control,” *Automatica*, 1993, 29(1):201-203.

- [8] Inoannou, P. A. and Jing, S., *Robust Adaptive Control*, Prentice-Hall International, Inc. 1996.
- [9] Zames, G., “Feedback and optimal sensitivity: model reference transformations, multiplicative seminorms, and approximate inverse,” *IEEE Trans. Automat. Contr.*, 1981, 26(4):301-320.
- [10] Francis, B. A., *A course in control theory. Lecture notes in control and information sciences*, Berlin:Springer-Verlag, 1987.
- [11] Doyle, J. C. et al., “State-space solutions to standard H_2 and H_∞ control problems,” *American control conference*, Atlanta, 1988.
- [12] Doyle, J. C. et al., “State-space solutions to standard H_2 and H_∞ control problems,” *IEEE Trans. Automatic Control*, 1989, 34(2):831-847.
- [13] Zhou, K. and Khargonekar, P., “Robust stabilization of linear systems with norm-bounded time-varying uncertainty,” *Syst. Contr. Letters*, 1988, 10(1):17-20.
- [14] Nielsen, Agnar Kenneth Nygaard, “Helicopter dynamics and robust control,” 2005.
- [15] Isidori, A., Marconi, L., and Serrani, A., “Robust nonlinear motion control of a helicopters,” *IEEE Transaction on Automatic Control*, vol. 48, no. 3, pp. 413-426, 2003.
- [16] Bobby, R. I., Mansor, H., Gunawan, T. S. and Khan, S., “Robust adaptive LQR control of nonlinear system application to 3-DOF flight control system,” *IEEE International Conference on Smart Instrumentation, Measurement and Applications (ICSIMA)*, Kuala Lumpur, 2014, pp. 1-4.

- [17] Vilela Lopes, R. and Milhan, A., “Modeling and Constrained Predictive Control of a 3DOF Helicopter,” 2006.
- [18] Ljung, L. and Söderström, S., *Theory and Practice of Recursive Identification*, Cambridge: MIT Press, 1983, pp. 122-130.
- [19] LABORATORY GUIDE: 3 DOF Helicopter Experiment for LabVIEW Users, Quanser Inc, Markham, Canada, 2012.
- [20] NI.com, “PCIe-6321 Multifunction I/O Device,” 2017. [Online]. Available: <http://www.ni.com/en-us/support/model.pcie-6321.html>. [Accessed: 23-Aug-2017].
- [21] Logitech.com, “ATTACK 3 JOYSTICK SUPPORT,” 2017. [Online]. Available: http://support.logitech.com/en_us/product/attack-3-joystick. [Accessed: 23-Aug-2017].
- [22] Skogestad, S. and Postlethwaite, I., *Multivariable feedback control*, Chichester: Wiley, 2010, pp. 293.
- [23] Skogestad, S. and Postlethwaite, I., *Multivariable feedback control*. Chichester: Wiley, 2010, pp. 353-361.
- [24] mathworks.com, “hinsyn,” 2017. [Online]. Available: <https://www.mathworks.com/help/robust/ref/hinsyn.html>. [Accessed: 25-Aug-2017].

Vita

Shuai Yue, son of Lan He and Hanzeng Yue, was born in Beijing, China on May 15, 1992. He received his Bachelor of Science degree in Mechanical Engineering from Shanghai Jiaotong University in June 2015. From 2016 to 2017 he worked at Lehigh University toward his Masters of Science degree under Prof. E. Schuster in the Interdisciplinary Automatic Controls Laboratory.